J. Fluid Mech. (2007), *vol.* 575, *pp.* 221–255.
doi:10.1017/S0022112006004277 Printed in the United Kingdom

Effects of heat release on turbulent shear flows. Part 3. Buoyancy effects due to heat release in jets and plumes

FRANCISCO J. DIEZ† AND WERNER J. A. DAHM

Laboratory for Turbulence & Combustion (LTC), Department of Aerospace Engineering, The University of Michigan, Ann Arbor, MI 48109-2140, USA

(Received 21 May 2006 and in revised form 3 September 2006)

An integral method is presented for determining effects of buoyancy due to heat release on the properties of reacting jets and plumes. This method avoids the Morton entrainment hypothesis entirely, and thus removes the ad hoc 'entrainment modelling' required in most other integral approaches. We develop the integral equation for the local centreline velocity $u_c(x)$, which allows modelling in terms of the local flow width $\delta(x)$. In both the momentum-dominated jet limit and buoyancy-dominated plume limit, dimensional arguments show $\delta(x) \sim x$, and experimental data show the proportionality factor c_δ to remain constant between these limits. The entrainment modelling required in traditional integral methods is thus replaced by the observed constant c_δ value in the present method. In non-reacting buoyant jets, this new integral approach provides an exact solution for $u_c(x)$ that shows excellent agreement with experimental data, and gives simple expressions for the virtual origins of jets, plumes and buoyant jets. In the exothermically reacting case, the constant c_δ value gives an expression for the buoyancy flux $B(x)$ that allows the integral equation for $u_c(x)$ to be solved for arbitrary exit conditions. The resulting $u_c(x)$ determines the local mass, momentum and buoyancy fluxes throughout the flow, as well as the centreline mixture fraction $\zeta_c(x)$ and thus the flame length L. The latter provides the proper parameters Ω and Λ that determine buoyancy effects on the flame, and provides power-law scalings in the momentum-dominated and buoyancy-dominated limits. Comparisons with buoyant flame data show excellent agreement over a wide range of conditions.

1. Introduction

Bridging the gap between fluid dynamics and combustion science requires an understanding of how heat released in exothermic chemically reacting turbulent shear flows alters the entrainment and mixing properties relative to a non-reacting flow under otherwise identical conditions. A fundamentally based general equivalence principle, applicable to mixing-limited reacting flows (Tacina & Dahm 2000; hereinafter referred to as Part 1), has been shown to allow heat release effects on shear flows to be deduced from the scaling laws that govern the corresponding non-reacting flow. When applied to turbulent jets, this equivalence principle was shown in Part 1 to predict accurately the effects of heat release in the near and far fields of planar

† Present address: Department of Mechanical Engineering, Rutgers University, Piscataway, NJ, USA.

and axisymmetric turbulent jet flames under conditions for which buoyancy effects are negligible. This same principle was also shown (Dahm 2005, hereinafter referred to as Part 2) to predict correctly the fundamentally different effects of heat release on the properties of turbulent mixing layers when buoyancy effects can be neglected. The present paper addresses the effects of buoyancy in exothermic reacting turbulent jets, plumes and buoyant jets. It uses the equivalence principle relating non-reacting and exothermic reacting shear flows to develop a simple integral method that determines buoyancy effects in such flows via the change in total buoyancy flux with downstream distance throughout the flow.

Reacting jets and plumes differ from most other combustion systems by the large buoyancy forces that can act on the flow due to heat release. Unlike simple non-reacting plumes, for which the total buoyancy flux is constant, in reacting flows, the buoyancy flux can increase dramatically owing to heat release along the length of the flame. The resulting variation in buoyancy flux can produce large changes in the flow properties and the flame length relative to the corresponding flow with constant buoyancy flux. Integral methods based on various approximations have been widely used to account for the evolving flow properties in such exothermic reacting jets, plumes and related flows (e.g. Steward 1970; Heskestad 1981; Zukoski, Kubota & Cetegen 1981; Cetegen, Zukoski & Kubota 1984; Peters & Göttgens 1991; Blake & McDonald 1995; Blake & Coté 1999; Kaminski, Tait & Carazzo 2005). In all such integral methods, the partial differential equations for conservation of mass, momentum, and energy are integrated across the flow, together with self-similar forms for the lateral profiles of velocity and density, to provide simple ordinary differential equations for various integral flow properties such as the mass flux $m(x)$, momentum flux $J(x)$ and buoyancy flux $B(x)$. These integral equations can be readily solved with certain modelling approximations to determine the resulting changes in flow properties with increasing downstream distance x.

Most integral methods to date for buoyant jets and plumes have been based on an approximation widely referred to as the 'Morton entrainment hypothesis', introduced by Morton, Taylor & Turner (1956) (see also Morton 1958; List 1982; Turner 1986). This can be written in various forms that amount to a representation of the local mass entrainment rate into the flow as $\mathrm{d}m/\mathrm{d}x \sim \alpha m(x)/\delta(x)$, where $m(x)$ is the local mass flux, $\delta(x)$ is the local self-similar profile width, and α is an 'entrainment coefficient'. Measurements in non-reacting flows have shown that such an entrainment coefficient would need to vary from $\alpha \approx 0.057$ in momentum-dominated jets having negligible buoyancy, to $\alpha \approx 0.082$ in plumes driven entirely by buoyancy (e.g. Gebhart *et al.* 1988; Linden 2000). As a result, α must be changed as the ratio of momentum and buoyancy varies along the flow. Lacking a fundamental basis on which to model this entrainment coefficient, integral methods based on the Morton entrainment hypothesis represent the local value of α by various *ad hoc* expressions in terms of the Froude number. Numerous such models for α have been proposed, as summarized by Gebhart *et al.* (1988), and the various integral methods differ largely by their choice for the 'entrainment model' for α (e.g. Teixeira & Miranda 1997; Kaminski *et al.* 2005). Chen & Rodi (1980) do not present an integral method *per se*, but use the integral equations to develop requirements for self-similarity in buoyant jets.

Here we develop an approach that avoids the Morton entrainment hypothesis altogether, and thereby removes the need for such ad hoc 'entrainment modelling'. Rather than working in terms of an integral equation for $\mathrm{d}m/\mathrm{d}x$, we use the integral equation for the momentum flux $\mathrm{d}J/\mathrm{d}x$ to develop a corresponding equation for the local centreline velocity $u_c(x)$. This has the advantage that the modelling can

be done in terms of the local flow width $\delta(x)$, for which dimensional considerations require the far-field scaling $\delta \sim x$ in both the momentum-dominated jet limit and the buoyancy-dominated plume limit, and for which experimental data further show that the proportionality constant c_δ remains unchanged in the far field from the jet limit to the plume limit (Papanicolaou & List 1988). Thus, whereas α varies between these two limits and must be modeled, c_δ is invariant between these limits and thus can be represented by a single constant without any further modelling. In effect, the ad hoc entrainment modelling required in traditional integral methods is replaced in the present approach by the observed constant value of c_δ. The present results are solely applicable to the far field, where only the source momentum flux J_0 or source buoyancy flux B_0 remain relevant, and where thus $\delta \sim x$ follows immediately from dimensional considerations; entrainment models in some traditional integral methods allow a represention of the flow in the near field, where the far-field scaling $\delta \sim x$ does not apply.

In non-reacting buoyant jets, for which $B(x)$ is constant, the present integral approach is found to give an exact solution for the centreline velocity $u_c(x)$. This solution is simpler than that obtained by Morton (1958) from the entrainment hypothesis, it avoids an ad hoc entrainment model, and it is seen herein to provide excellent agreement with buoyant jet data. Moreover, the present solution also provides a simple expression for the virtual origin of buoyant jets, as well as for the pure jet and pure plume limits.

In exothermically reacting buoyant jet flames, for which the buoyancy flux B(x) increases along the length of the flame, the data of Papanicolaou & List (1988) that show c_δ to be independent of buoyancy allows the constant c_δ value to be introduced in the integral equation for $\mathrm{d}B/\mathrm{d}x$. This gives a simple expression for $B(x)$ in terms of the centreline velocity $u_c(x)$. Introducing this in the integral momentum equation then provides a simple integral equation for $u_c(x)$ that can be solved for arbitrary exit conditions. The resulting $u_c(x)$ then determines the mass flux $m(x)$, the momentum flux $J(x)$ and the buoyancy flux $B(x)$ throughout the flow. The mass flux in turn determines the centreline mixture fraction $\zeta_c(x)$, which determines the flame length L in terms of the reaction stoichiometry. Comparisons with data for centreline velocity decay and flame length in buoyant jet flames show good agreement over a wide range of flame conditions. Moreover, the resulting flame length expression provides the proper parameters that characterize the extent to which buoyancy effects are significant throughout the flame.

From these results, it will be seen herein that, when the inertial effects of the reduced densities due to heat release have been properly accounted for by the equivalence principle of Parts 1 and 2, then even the effects of buoyancy produced by heat release can be directly obtained from the scaling laws for the corresponding non-reacting flow under otherwise identical conditions. The essential fundamental change produced in the flow by heat release is thus the inertial change resulting from the reduced density. Once this inertial effect has been accounted for by the equivalence principle, then secondary effects of heat release, including buoyancy effects, follow directly from the scaling laws that govern the non-reacting flow. The equivalence principle thus allows scaling laws for exothermic reacting flows to be directly obtained from the scaling laws for non-reacting flows.

The paper is organized as follows. Section 2 lays out essential preliminaries and gives the scalings for δ and u_c in the jet and plume limits. Section 3 then develops the integral method for buoyant jets and obtains the exact solution for the non-reacting case. Section 4 extends the integral method to the exothermic reacting case, and then

examines parametric effects of heat release in buoyant jet flames and compares results from the integral method with measured values. Section 5 derives the criterion for the flame length in the integral method, and compares the resulting predicted flame lengths with measured values from buoyant jet flames. Section 6 discusses implications of this integral method for understanding heat release effects on the flame length and combustion properties of buoyant flames.

2. Scaling in the jet and plume limits

The principal aim of this paper is to clarify the far-field scaling of exothermic reacting turbulent buoyant jets, for which the buoyancy flux $B(x)$ increases along the downstream distance x owing to combustion heat release. However, since the local value of $\mathrm{d}B/\mathrm{d}x$ is set by the rate of heat release within the flow, which in turn is determined by the rate of entrainment $\mathrm{d}m/\mathrm{d}x$ into the flow, the resulting coupling makes the exothermic reacting flow scaling significantly non-trivial. There are, however, limit cases in which the scaling can be readily obtained, which provide the starting point for the present integral method for the complete problem. In this section, we thus first consider the non-reacting limit and develop the momentum-dominated jet scaling and the buoyancy-dominated plume scaling. These then provide the basis for the integral method for non-reacting turbulent buoyant jets developed in § 3, which in turn leads to the integral method for exothermic reacting turbulent buoyant jets in § 4.

2.1. *Mass, momentum and buoyancy fluxes*

As indicated in figures 1 and 2, the flow in the self-similar far field produced by any finite-area source, through which issue exit values of the mass, momentum and buoyancy fluxes, respectively denoted m_E, J_E and B_E, can be equivalently represented by a point source at $x=0$ having source momentum flux J_0 and buoyancy flux B_0, but with the source mass flux $m_0 \equiv 0$. Through proper choice of the source values J_0 and B_0, and the exit value x_E, the flow produced by the point source will have $m(x_E)=m_E$, $J(x_E)=J_E$ and $B(x_E)=B_E$, and thus, at sufficiently large downstream distances x, will be identical to the flow produced by the actual finite-area source.

At any downstream location x from the source, the local mass flux $m(x)$, momentum flux $J(x)$, and buoyancy flux $B(x)$ are given by

$$m(x) \equiv \int_0^\infty \overline{\rho u}(x,r) 2\pi r \,\mathrm{d}r, \tag{1a}$$

$$J(x) \equiv \int_0^\infty \overline{\rho u^2}(x,r) 2\pi r \,\mathrm{d}r, \tag{1b}$$

$$B(x) \equiv \int_0^\infty g\overline{\Delta\rho u}(x,r) 2\pi r \,\mathrm{d}r, \tag{1c}$$

where $\Delta\rho(x,r) \equiv \rho_\infty - \rho(x,r)$. The corresponding exit values are denoted m_E, J_E and B_E. Thus for a source with exit area A_E, uniform exit velocity U_E and uniform exit density ρ_E the exit values are

$$m_E = \rho_E U_E A_E, \tag{2a}$$

$$J_E = \rho_E U_E^2 A_E, \tag{2b}$$

$$B_E = g\Delta\rho_E U_E A_E. \tag{2c}$$

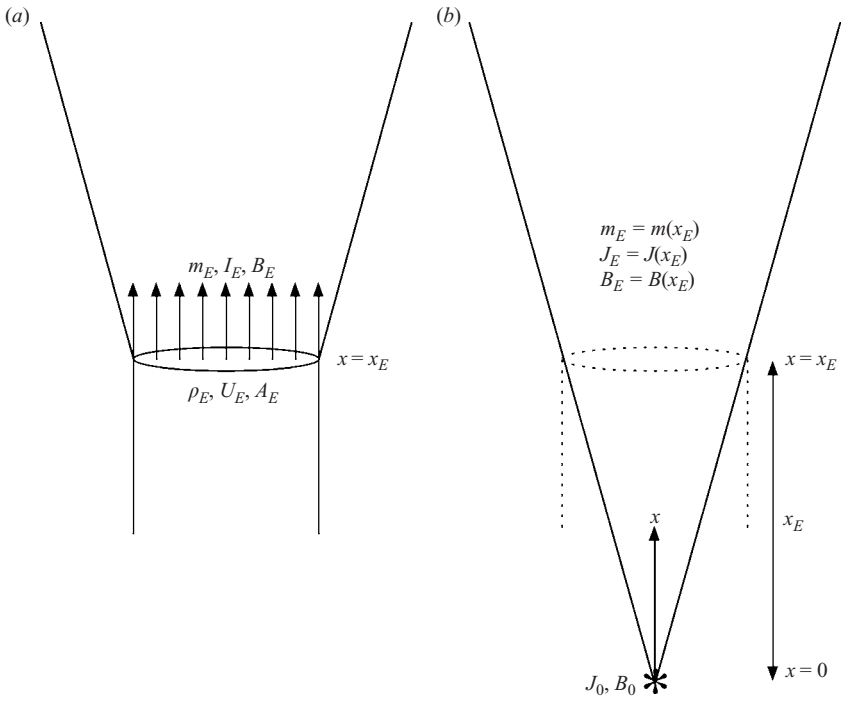

FIGURE 1. Representation of (*a*) an actual finite-area source by (*b*) an equivalent ideal point source at $x \equiv 0$ upstream of the exit plane, with the source mass flux $m_0 \equiv 0$ and with the source momentum flux J_0 and buoyancy flux B_0, chosen to match the exit values m_E, J_E and B_E at $x = x_E$ via (11) for jets, (16) for plumes, and (47) for buoyant jets.

For non-uniform exit conditions, m_E, J_E and B_E are obtained by integrating in (1*a*)–(1*c*) over the exit area. At sufficiently large downstream distances x from the source, $m(x) \gg m_E$ and thus most of the fluid moving with the flow has been entrained from the surrounding medium. As a consequence, the density ρ is approximately equal to the effective surrounding fluid density ρ_∞^{eff} of Part 1, where in the non-reacting case $\rho_\infty^{eff} \equiv \rho_\infty$ and in the exothermic reacting case ρ_∞^{eff} is given by (3*b*) or (4*b*) in Part 1. In this 'far field', the mean streamwise velocity and density-difference profiles in the non-reacting flow are self-similar in the scaled radial coordinate $\eta \equiv r/\delta(x)$, with the profile shapes being approximately Gaussian and given by

$$\frac{\overline{u}(x,r)}{u_c(x)} = f(\eta) \text{ where } f(\eta) \approx \exp(-a_f \eta^2), \tag{3a}$$

$$\frac{\overline{\Delta\rho}(x,r)}{\Delta\rho_c(x)} = h(\eta) \text{ where } h(\eta) \approx \exp(-a_h \eta^2). \tag{3b}$$

Here $u_c(x)$ denotes the local mean centreline velocity, $\delta(x)$ is the local profile width, as indicated in figure 2, and is the mean centreline density difference. The constant a_f in (3*a*) results from the choice of δ, here defined as the full width at which the mean velocity has decreased to 5 % of its centreline value, while a_h in (3*b*) is obtained from Papanicolaou & List (1988), giving

$$a_f = 12.0, \tag{4a}$$

$$a_h = 10.7. \tag{4b}$$

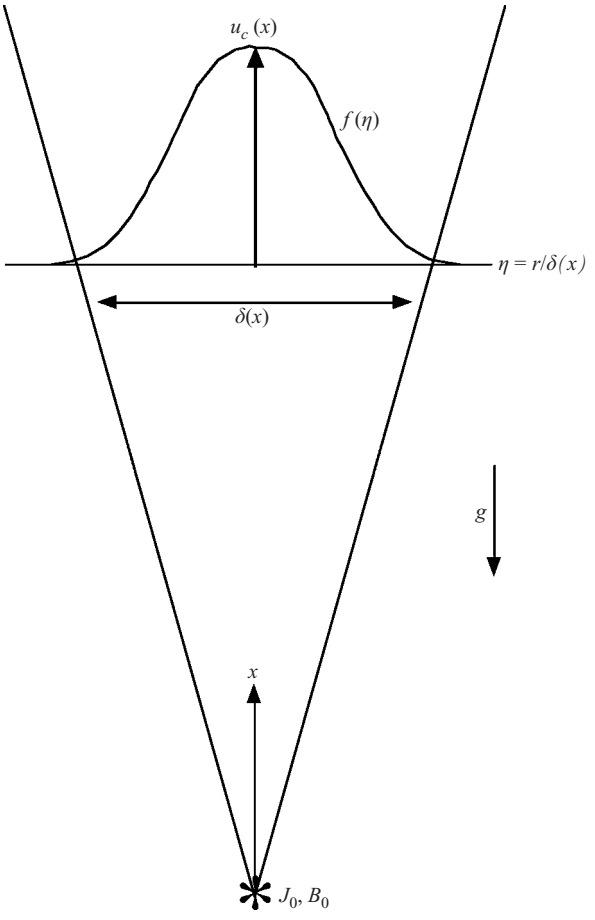

FIGURE 2. Self-similar far field of axisymmetric turbulent buoyant jets, showing the local flow width $\delta(x)$ and centreline velocity $u_c(x)$ from the mean velocity profile $f(\eta)$.

From (3) and (4) various integrals that arise in the analysis below can be evaluated as

$$I_1 = \int_0^\infty f(\eta) 2\pi\eta \, \mathrm{d}\eta = \frac{\pi}{a_f} \approx 0.262, \tag{5a}$$

$$I_2 = \int_0^\infty f^2(\eta) 2\pi\eta \, \mathrm{d}\eta = \frac{\pi}{2a_f} \approx 0.131, \tag{5b}$$

$$I_3 = \int_0^\infty f(\eta) 2\pi\eta \, \mathrm{d}\eta = \frac{\pi}{a_h} \approx 0.294, \tag{5c}$$

$$I_4 \equiv \int_0^\infty f(\eta) h(\eta) 2\pi\eta \, \mathrm{d}\eta = \frac{\pi}{(a_f + a_h)} \approx 0.138. \tag{5d}$$

From (1)–(5), the mass flux $m(x)$, momentum flux $J(x)$ and buoyancy flux $B(x)$ are given in terms of $u_c(x)$, $\delta(x)$ and $\Delta\rho_c(x)$ as

$$m(x) \approx I_1 \rho_\infty u_c(x) \delta^2(x), \tag{6a}$$

$$J(x) \approx I_2 \rho_\infty u_c^2(x) \delta^2(x), \tag{6b}$$

$$B(x) \approx I_4 g \Delta\rho_c(x) u_c(x) \delta^2(x). \tag{6c}$$

The expressions in (6*a*)–(6*c*) provide the starting point for the integral method developed herein. Note that fluctuation correlations in (1*a*)–(1*c*), which have for clarity been omitted in (5*a*)–(5*d*), lead only to comparatively small changes in I_1–I_4 which are accounted for as shown below.

2.2. *The jet limit*

2.2.1. *Scaling laws for $\delta(x)$ and $u_c(x)$*

The term 'jet' refers to the flow produced by an ideal point source of axial momentum for which the source mass flux is zero, namely $m_0 \equiv 0$, and the local buoyancy flux is zero throughout the flow, namely $B(x) \equiv 0$. Since no buoyancy acts on the fluid, the momentum flux $J(x)$ at all downstream distances x must remain constant at the source value J_0. The source momentum flux is then the only integral invariant of the flow, and thus in the self-similar far field the local flow width $\delta(x)$ and the local mean centreline velocity $u_c(x)$ can depend only on J_0, the downstream distance x and the ambient fluid density ρ_∞. As a result, on dimensional grounds the scalings for δ and u_c in jets must be

$$\delta \sim x, \tag{7a}$$

$$u_c \sim (J_0/\rho_\infty)^{1/2} x^{-1}, \tag{7b}$$

with the consequence that the proportionality constants c_δ and c_u in (7*a*) and (7*b*) must be the same for all jets. Measurements in jets (e.g. Papanicolaou & List 1988) have shown these scaling constants to be

$$(c_\delta)_j \approx 0.36, \tag{8a}$$

$$(c_u)_j \approx 7.2, \tag{8b}$$

where the subscript 'j' denotes constants applicable to the jet-limit scaling. From (6*a*), (7) and (8), the resulting mass flux scaling in jets is thus

$$m(x) = I_1 (c_u)_j (c_\delta)_j^2 (\rho_\infty J_0)^{1/2} x. \tag{9}$$

For later reference in relation to exothermic reacting buoyant jet flames, figure 10 of Part 1 shows experimental data from numerous far-field studies of highly exothermic jet flames, where $\Delta\rho/\rho_\infty$ is not small. Those data confirm that even when $\Delta\rho/\rho_\infty$ is large, the $\delta \sim x$ far-field scaling in (7*a*) applies with the same c_δ as in (8*a*) found by Papanicolaou & List (1988) for small $\Delta\rho/\rho_\infty$. The interpretation that non-small values of $\Delta\rho/\rho_\infty$ may lead to departures from $\delta = c_\delta x$ is attributable to the fact that, in most non-reacting buoyant jet experiments, large $\Delta\rho/\rho_\infty$ values occur only near the jet source, where the far-field scaling $\delta \sim x$ does not apply. Such departures from the scaling in (7*a*) and (8*a*) are thus due to near-field effects, and not an effect of non-small $\Delta\rho/\rho_\infty$ in the far field, where the present method applies.

2.2.2. *The virtual origin x_E*

The results in (7)–(9) are for the flow produced by an ideal point source at $x \equiv 0$, namely one that introduces momentum flux J_0 but no source mass flux; i.e $m_0 \equiv 0$. However, real jets are typically produced by finite-area sources that introduce a non-zero exit mass flux m_E when producing the exit momentum flux J_E. Proper account must be taken to relate the exit values m_E and J_E to the point source values m_0 and J_0 via the virtual origin.

Figure 1 shows the basic principle involved in determining the effective distance x_E of the finite-area exit from the ideal equivalent point source, often termed the 'virtual

origin'. If x is measured from the ideal point source, then x_E is the downstream distance at which the resulting mass flux $m(x_E) = m_E$ and the resulting momentum flux $J(x_E) = J_E$. The latter is automatically satisfied, since in jets the momentum flux $J(x) \equiv J_0$, and thus the appropriate value of J_0 for the point source to produce the same flow as the actual source is $J_0 = J_E$. Matching the resulting mass flux $m(x_E)$ from (9) to the actual exit mass flux m_E then requires

$$m_E = I_1 (c_u)_j (c_\delta)_j^2 (\rho_\infty J_0)^{1/2} x_E, \tag{10}$$

from which

$$x_E = \frac{\sqrt{\pi}/2}{I_1 (c_u)_j (c_\delta)_j^2} \underbrace{\left[\frac{2 m_E}{(\pi \rho_\infty J_E)^{1/2}} \right]}_{\equiv d^*}. \tag{11}$$

Thus x_E in (11) ensures that, for the jet limit, $m(x_E) = m_E$ and $J(x_E) = J_E$. For the values of I_1, $(c_u)_j$ and $(c_\delta)_j$ in (5*a*), (8*a*) and (8*b*), this gives the virtual origin for jets as $x_E \approx 3.6 d^*$, where d^* is the 'far-field equivalent source diameter'. From its definition in (11), the equivalent diameter for a circular nozzle with uniform exit density ρ_E and velocity U_E leads to the classical result $d^* = (\rho_E / \rho_\infty)^{1/2} d_E$.

When, as is common in practice, x is used to denote the downstream distance measured from the exit of the finite-area source, rather than the distance from the ideal point source, then x in (7)–(9) must be replaced by $x + x_E$ as figures 1 and 2 indicate, with x_E from equation (11).

2.3. *The plume limit*

2.3.1. *Scaling laws for $\delta(x)$ and $u_c(x)$*

A 'plume' is produced by a point source for which the source mass and momentum fluxes are both zero, namely $m_0 \equiv 0$ and $J_0 \equiv 0$, with the flow created instead by the buoyancy flux B_0 introduced by the source. The positive buoyancy that acts on the fluid causes the momentum flux $J(x)$ to increase with x. In the absence of reaction heat release or other effects that change the total buoyancy flux B, the source buoyancy flux B_0 is then the only integral invariant of the flow. Thus in the self-similar far field, the local flow width $\delta(x)$ and the local mean centreline velocity $u_c(x)$ can depend only on B_0, the downstream distance x, and the ambient fluid density ρ_∞. On dimensional grounds, the scalings for δ and u_c in plumes must thus be

$$\delta \sim x, \tag{12a}$$

$$u_c \sim (B_0 / \rho_\infty)^{1/3} x^{-1/3}. \tag{12b}$$

The proportionality constants c_δ and c_u in the far-field scalings in (12) must then be the same for all plumes, and from Papanicolaou & List (1988) are found to be

$$(c_\delta)_p \approx 0.36, \tag{13a}$$

$$(c_u)_p \approx 4.0, \tag{13b}$$

where the subscript 'p' denotes constants applicable to the plume-limit scaling. For later reference, from (6*a*), (6*b*), (12) and (13) the resulting mass and momentum flux scalings in plumes are thus

$$m(x)/\rho_\infty \approx I_1 (c_u)_p (c_\delta)_p^2 (B_0/\rho_\infty)^{1/3} x^{5/3}, \tag{14a}$$

$$J(x)/\rho_\infty \approx I_2 (c_u)_p^2 (c_\delta)_p^2 (B_0/\rho_\infty)^{2/3} x^{4/3}, \tag{14b}$$

As noted in § 2.2.1, even when the local density difference is not small, the $\delta \sim x$ far-field scaling in (12*a*) still applies with the same c_δ as in (13*a*). The common interpretation that large values of $\Delta\rho/\rho_\infty$ lead to deviations from this scaling is due to the fact that, in most non-reacting plume experiments, large $\Delta\rho/\rho_\infty$ values occur only near the jet source, where the far-field scaling $\delta \sim x$ does not apply. Departures from the scaling in (12*a*) and (13*a*) then result from near-field effects, and are not a result of $\Delta\rho/\rho_\infty$ in the far field where the present method applies.

2.3.2. *The virtual origin* x_E

The results in (12)–(14) are for plumes produced by an ideal point source at $x \equiv 0$ that introduces buoyancy flux B_0 but no mass flux; i.e. $m_0 \equiv 0$. However, real plumes are typically created by finite-area sources that produce an exit mass flux m_E and an associated exit momentum flux J_E in producing the exit buoyancy flux B_E. A properly chosen virtual origin x_E must therefore be introduced to match the mass and momentum fluxes $m(x_E)$ and $J(x_E)$ to the exit values m_E and J_E.

Figure 1 again serves to show the basic principle involved. If x is measured from the ideal point source, then x_E is the value at which the resulting mass flux $m(x_E) = m_E$ and $B(x_E) = B_E$. The latter is automatically satisfied, since in plumes $B(x) \equiv B_0$, and thus the buoyancy flux required for the point source to produce the same flow as the actual source is $B_0 = B_E$. From (14*a*) the mass flux matching $m(x_E) = m_E$ requires

$$(m_E/\rho_\infty) \approx I_1(c_u)_p(c_\delta)_p^2(B_0/\rho_\infty)^{1/3}x_E^{5/3}, \tag{15}$$

from which the virtual origin is

$$x_E = \left(\frac{1}{I_1(c_u)_p(c_\delta)_p^2}\right)^{3/5}\left[\frac{(m_E/\rho_\infty)^{3/5}}{(B_E/\rho_\infty)^{1/5}}\right]. \tag{16}$$

It may be readily verified that matching the momentum flux $J(x_E)$ in (14*b*) to the exit value J_E gives the same result for the virtual origin as in (16). Thus, x_E in (16) ensures that $m(x_E) = m_E$, $J(x_E) = J_E$, and $B(x_E) = B_E$.

When, as is often the case, x is used to denote the downstream distance measured from the exit of the finite source, rather than the distance from the ideal point source, then x in (12)–(14) must be replaced by $x + x_E$, with x_E from (16).

3. Scaling of buoyant jets

As a further step in developing the scaling for exothermically reacting turbulent buoyant jets in § 4, we now use the results from § 2 to determine the scaling for non-reacting buoyant jets. The term 'buoyant jet' denotes the flow produced by a point source that introduces both an initial momentum flux J_0 and initial positive buoyancy flux B_0; Morton (1958) refers to such flows as 'forced plumes'. In the absence of heat release, the local buoyancy flux $B(x)$ remains constant at B_0 for all downstream distances x, but the momentum flux $J(x)$ will increase as a result of the buoyancy that acts on the fluid. In this section, we develop an integral method for such buoyant jets and obtain an exact solution for the case of non-reacting buoyant jets.

3.1. *Scaling parameters for buoyant jets*

Since buoyant jets have one additional source parameter (either B_0 or J_0) relative to the jet or plume limits in § 2, on dimensional grounds the scalings for δ and u_c must involve an additional length scale l^* and an additional velocity scale u^*. These are, in turn, the only such quantities that can be formed from J_0, B_0 and ρ_∞, and therefore

must be

$$l^* \equiv \frac{(J_0/\rho_\infty)^{3/5}}{(B_0/\rho_\infty)^{1/2}}, \tag{17a}$$

$$u^* \equiv \frac{(B_0/\rho_\infty)^{1/2}}{(J_0/\rho_\infty)^{1/4}}. \tag{17b}$$

Note that l^* is sometimes referred to as the 'Morton length scale', and we will thus also refer to u^* as the 'Morton velocity scale'. On dimensional grounds, the resulting scalings for δ and u_c in buoyant jets must thus be

$$\frac{\delta(x)}{l^*} = f_1(\chi), \tag{18a}$$

$$\frac{u_c(x)}{u^*} = f_2(\chi), \tag{18b}$$

$$\chi \equiv \frac{x}{l^*}. \tag{18c}$$

The functions f_1 and f_2 must recover the jet-limit scaling as $B_0 \to 0$, for which $l^* \to \infty$ and thus $\chi \to 0$, and recover the plume-limit scaling as $J_0 \to 0$, for which $l^* \to 0$ and thus $\chi \to \infty$. As a result, in the jet limit $\chi \to 0$ the scalings in (7a) and (7b) require

$$f_1(\chi) \to (c_\delta)_j \chi, \tag{19a}$$

$$f_2(\chi) \to (c_u)_j \chi^{-1}, \tag{19b}$$

while in the plume limit $\chi \to \infty$ the scalings in (12a) and (12b) require

$$f_1(\chi) \to (c_\delta)_p \chi, \tag{20a}$$

$$f_2(\chi) \to (c_u)_p \chi^{-1/3}. \tag{20b}$$

3.2. *The flow width* $(\delta/l^*) = f_1(\chi)$

Comparing (19a) and (20a) it is apparent that in buoyant jets the flow width has the same scaling $f_1(\chi) \sim \chi$ in both the jet and plume limits, and from (8a) and (13a) even the proportionality constant c_δ is the same in both limits. Moreover, measurements in non-reacting buoyant jets (Papanicolaou & List 1988; see also Kotsovinos & List 1977) show that c_δ remains constant at this same value for all χ between the jet and plume limits. This is consistent with the finding by Chen & Rodi (1980) that $\delta \sim x$ is a requirement for self-similarity. Thus for all χ

$$f_1(\chi) = c_\delta \cdot \chi, \tag{21}$$

from which for all x

$$\delta \approx c_\delta x, \tag{22a}$$

with

$$c_\delta \approx 0.36. \tag{22b}$$

The invariance of c_δ in (22a) and (22b) between the jet and plume limits will be seen to here replace the *ad hoc* modelling of an 'entrainment coefficient' α used in most other integral approaches for buoyant jets and plumes.

3.3. *The centreline velocity* $(u_c/u^*) = f_2(\chi)$

With $\delta(x)$ in (22), the integral equation for the momentum flux $J(x)$ allows a corresponding integral equation for the centreline velocity $u_c(x)$ in terms of the buoyancy flux $B(x)$.

3.3.1. *Integral form of the momentum equation*

The local rate of change of axial momentum results from the buoyancy body force as

$$\frac{\mathrm{d}}{\mathrm{d}x}[\rho u^2(x,r)] = g\Delta\rho(x,r), \tag{23}$$

from which

$$\frac{\mathrm{d}}{\mathrm{d}x}\int_0^\infty \rho u^2 2\pi r\,\mathrm{d}r = \int_0^\infty g\Delta\rho(x,r)2\pi r\,\mathrm{d}r. \tag{24}$$

From (1*b*) and (1*c*) this becomes

$$\frac{\mathrm{d}}{\mathrm{d}x}J(x) = \frac{B(x)}{u_c(x)}\frac{\displaystyle\int_0^\infty h(\eta)2\pi\eta\,\mathrm{d}\eta}{\displaystyle\int_0^\infty f(\eta)h(\eta)2\pi\eta\,\mathrm{d}\eta}, \tag{25}$$

from which

$$\frac{1}{J}\frac{\mathrm{d}J}{\mathrm{d}x} = (I_3/I_4)\frac{1}{J(x)}\frac{B(x)}{u_c(x)}. \tag{26}$$

From (6*b*) and (22)

$$J(x) = I_2 c_\delta^2 \rho_\infty u_c^2(x)x^2, \tag{27}$$

and thus the left-hand side of (26) can be expressed as

$$\frac{1}{J}\frac{\mathrm{d}J}{\mathrm{d}x} = \frac{2}{u_c}\frac{\mathrm{d}u_c}{\mathrm{d}x} + \frac{2}{x}, \tag{28}$$

and the right-hand side of (26) can be expressed as

$$(I_3/I_4)\frac{1}{J(x)}\frac{B(x)}{u_c(x)} = 2\sigma\frac{(B(x)/\rho_\infty)}{u_c^3x^2}, \tag{29}$$

where

$$\sigma \equiv \frac{I_3}{2I_2I_4c_\delta^2}. \tag{30}$$

Substituting (28) and (29) into (26) thus gives a simple differential equation for $u_c(x)$ in terms of $B(x)$ as

$$\frac{\mathrm{d}u_c}{\mathrm{d}x} + \frac{u_c}{x} = \sigma\frac{(B(x)/\rho_\infty)}{u_c^2x^2}. \tag{31}$$

3.3.2. *Integration for $u_c(x)$ when $B(x) \equiv B_0$*

Up to this point in § 3 there has been no restriction on the buoyancy flux $B(x)$, and thus the integral momentum equation in (31) applies even in exothermic reacting buoyant jets, where $B(x)$ varies. However when, as in non-reacting buoyant jets, $B(x)$ remains constant at the source value B_0, then an exact solution for the centreline velocity $u_c(x)$ can be obtained from (31). Changing to the dimensionless centreline velocity and downstream coordinate

$$f_2(\chi) \equiv \frac{u_c}{u^*}, \qquad \chi \equiv \frac{x}{l^*}, \tag{32a, b}$$

when $B(x) \equiv B_0$, the integral equation in (31) becomes

$$\frac{\mathrm{d}f_2}{\mathrm{d}\chi} + \frac{f_2}{\chi} = \sigma(\chi f_2)^{-2}. \tag{33}$$

This is equivalent to

$$\mathrm{d}(\chi f_2)^3 = 3\sigma\chi\,\mathrm{d}\chi \tag{34}$$

which integrates to

$$f_2 = \frac{1}{\chi}\left[\tfrac{3}{2}\sigma\chi^2 + C\right]^{1/3}. \tag{35}$$

The integration constant C is found by taking the jet-limit $\chi \to 0$, in which (35) becomes

$$f_2 \to C^{1/3}\chi^{-1}. \tag{36}$$

Rewriting (36) in u_c and x via (32) gives

$$u_c \to C^{1/3}(J_0/\rho_\infty)^{1/2}x^{-1}, \tag{37}$$

and comparing with the jet scaling in (7*b*) and (8*b*) shows that

$$C = (c_u)_j^3. \tag{38}$$

As a check, note that taking the plume-limit $\chi \to \infty$ in (35) gives

$$f_2 \to \left(\tfrac{3}{2}\sigma\right)^{1/3}\chi^{-1/3}, \tag{39}$$

which can be rewritten in u_c and x via (32) to give

$$u_c \to \left(\tfrac{3}{2}\sigma\right)^{1/3}(B_0/\rho_\infty)^{1/3}x^{-1/3}. \tag{40}$$

Comparing (40) with the plume scaling in (12*b*) and (13*b*) shows that

$$\left(\tfrac{3}{2}\sigma\right) = (c_u)_p^3. \tag{41}$$

From (30) with (5*b*)–(5*d*) and (22*b*), (41) gives $(c_u)_p \approx 4.5$, which indeed compares acceptably with the value 4.0 in (13*b*); the difference is due to the relatively small contributions of the fluctuation correlations to I_n in (5), which as noted in § 2 have been omitted here for clarity, but will be accounted for as shown below.

Substituting (38) and (41) into (35) gives the centreline velocity in buoyant jets as

$$\frac{u_c(x)}{u^*} \equiv f_2(\chi) = \chi^{-1}\left[(c_u)_j^3 + (c_u)_p^3\chi^2\right]^{1/3} \quad \text{with } \chi \equiv \frac{x}{l^*}, \tag{42}$$

where u^* and l^* are from (17*a*) and (17*b*), and $(c_u)_j$ and $(c_u)_p$ are from (8*b*) and (13*b*). Note that using the measured value $(c_u)_p \approx 4.0$ given in (13*b*) from Papanicolaou & List (1988) in (42) in place of $(3\sigma/2)^{1/3}$ in (35) implicitly takes account of the contributions from the fluctuation correlations to the integrals in (1*a*)–(1*c*).

The result in (42) is an exact solution for the centreline velocity $u_c(x)$ in non-reacting turbulent buoyant jets that depends only on the observed constant value of c_δ in (21) and (22). This is compared in figure 3 with the measured centreline velocity decay data in buoyant jets of Papanicolaou & List (1988). It is apparent that for non-reacting buoyant jets, for which $B(x) \equiv B_0$, the solution in (42) to the present integral equation in (31) provides excellent agreement with measured values, and supports the present integral approach. In contrast to the solution of Morton *et al.*

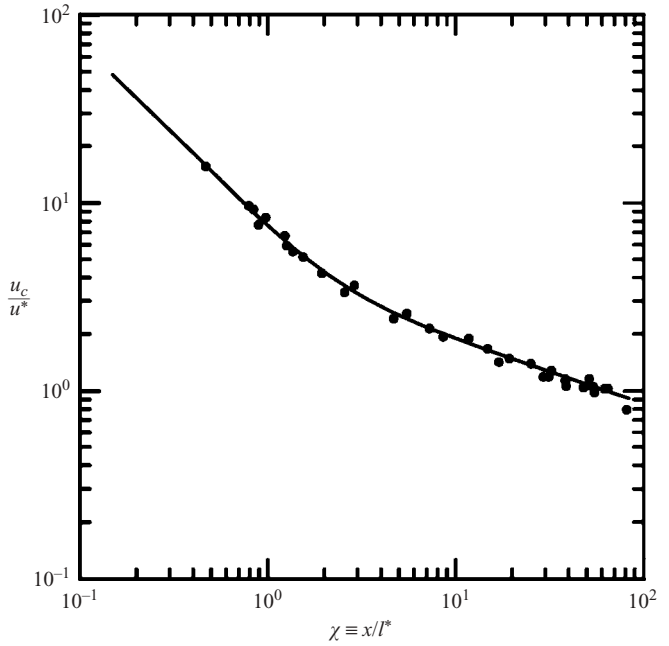

FIGURE 3. Verification of exact solution for centreline velocity $u_c(x)$ from present integral method for non-reacting ($B(x) \equiv B_0$) case, comparing the result in (42) (line) with experimental measurements of Papanicolaou & List (1988) (symbols). Note jet-limit scaling $f_2(\chi) \to (c_u)_j \chi^{-1}$ as $\chi \to 0$ and plume-limit scaling $f_2(\chi) \to (c_u)_p \chi^{-1/3}$ as $\chi \to \infty$.

(1956) and Morton (1958), the present approach effectively replaces *ad hoc* modelling of an entrainment coefficient α with the observed constant value of c_δ between the jet and plume limits.

3.4. *The source momentum flux J_0 and the virtual origin x_E*

The result in (42) is for the non-reacting flow produced by an ideal point source at $x \equiv 0$ that introduces momentum flux J_0 and buoyancy flux B_0 but no source mass flux; i.e. $m_0 \equiv 0$. Real buoyant jets produced by finite-area sources introduce a non-zero exit mass flux m_E in conjunction with the exit momentum flux J_E and exit buoyancy flux B_E. A properly chosen virtual origin x_E matches the mass flux $m(x_E)$ and momentum flux $J(x_E)$ produced by the point source to the exit mass and momentum fluxes m_E and J_E. In this case, both the virtual origin x_E and the appropriate source momentum flux J_0 must be determined, since $J(x_E) \neq J_0$.

Figure 1 again serves to show the basic principle involved. If x is measured from the ideal point source, then x_E is the value at which the resulting mass flux $m(x_E) = m_E$, the momentum flux $J(x_E) = J_E$, and the buoyancy flux $B(x_E) = B_E$. The latter requirement is automatically satisfied, since the buoyancy flux remains constant in the absence of heat release, and thus $B_0 = B_E$. The mass flux matching $m(x_E) = m_E$ requires from (6*a*) together with (17), (22), (32) and (42) that

$$m_E = I_I c_\delta^2 \rho_\infty \frac{(J_0/\rho_\infty)^{5/4}}{(B_0/\rho_\infty)^{1/2}} \chi_E \left[(c_u)_j^3 + (c_u)_p^3 \chi_E^2\right]^{1/3}, \tag{43}$$

from which

$$\chi_E\left[(c_u)_j^3+(c_u)_p^3\chi_E^2\right]^{1/3}=\frac{1}{I_I c_\delta^2}\frac{(m_E/\rho_\infty)(B_E/\rho_\infty)^{1/2}}{(J_0/\rho_\infty)^{5/4}},\tag{44}$$

where we have also made use of the fact that $B_0=B_E$. The source momentum flux J_0 on the right-hand side of (44) is unknown, but can be obtained from matching the momentum flux $J(x_E)=J_E$ This requires from (6*b*) together with (17), (22), (32) and (42) that

$$J_E=I_2c_\delta^2J_0\left[(c_u)_j^3+(c_u)_p^3\chi_E^2\right]^{2/3}.\tag{45}$$

Substituting from (44) for the bracketed term in (45) and rearranging gives

$$(J_0/\rho_\infty)=\left(\frac{I_2}{I_1^2c_\delta^2}\right)^{2/3}\frac{1}{\chi_E^{4/3}}\left[\frac{(m_E/\rho_\infty)^2(B_E/\rho_\infty)}{(J_E/\rho_\infty)}\right]^{2/3},\tag{46}$$

which may be substituted into (44) to determine the virtual origin ξ_E as

$$\chi_E=\left\{\left(\frac{I_1^2}{I_2^{5/2}c_\delta(c_u)_j^3}\right)\left[\frac{(J_E/\rho_\infty)^{5/2}}{(m_E/\rho_\infty)^2(B_E/\rho_\infty)}\right]-\left(\frac{(c_u)_p}{(c_u)_j}\right)^3\right\}.\tag{47}$$

For the given exit mass, momentum and buoyancy fluxes m_E, J_E and B_E of the finite-area source, (47) is first used to find the virtual origin χ_E. With this χ_E, (46) then gives the required momentum flux J_0 of the point source, which together with $B_0\equiv B_E$ then gives the Morton length and velocity scales, l^* and u^*, via (17*a*) and (17*b*). The resulting l^* together with χ_E then gives the virtual origin x_E. When, as is commonly done in practice, x is used to denote the downstream distance measured from the exit of the finite source, rather than the distance from the ideal point source, then x in (22) for $\delta(x)$ and in (42) for $u_c(x)$ must be replaced by $x+x_E$

Note, however, that (47) can become imaginary if J_E is below a minimum allowable value J^* given by

$$(J^*/\rho_\infty)=\left[\frac{I_2^{5/2}c_\delta(c_u)_p^3}{I_1^2}(m_E/\rho_\infty)^2(B_E/\rho_\infty)\right]^{2/5}.\tag{48}$$

For $J_E<J^*$, the resulting flow is in a class that Morton (1959) refers to as 'lazy plumes', for which J_E is too low, even for a pure plume, to be compatible with the combined values of m_E and B_E. In that case, the flow must initially be of a different type, as indicated in figure 4. The flow downstream of the exit plane at x_E does not begin to entrain ambient fluid until buoyancy has raised the momentum flux $J(x)$ to the minimum compatible value J^* for a plume. Beyond this point, denoted x^*, the resulting plume flow begins to entrain. A two-step procedure, related to that of Morton (1959) and Morton & Middleton (1973), may then be used to find the equivalent point source that produces the same flow for $x\gg x^*$ (see also Hunt & Kaye 2001). First note that the momentum equation in (26) may be equivalently written as

$$\frac{\mathrm{d}}{\mathrm{d}x}J^2(x)=2\left(\frac{I_2I_3}{I_1I_4}\right)B(x)m(x).\tag{49}$$

For $x<x^*$, the flow does not entrain, and thus $m(x<x^*)\equiv m_E$. Moreover, $B(x<x^*)\equiv B_E$ in the non-reacting case. For later reference, this applies even in the exothermic reacting case since, owing to the absence of entrainment over $x<x^*$, essentially no

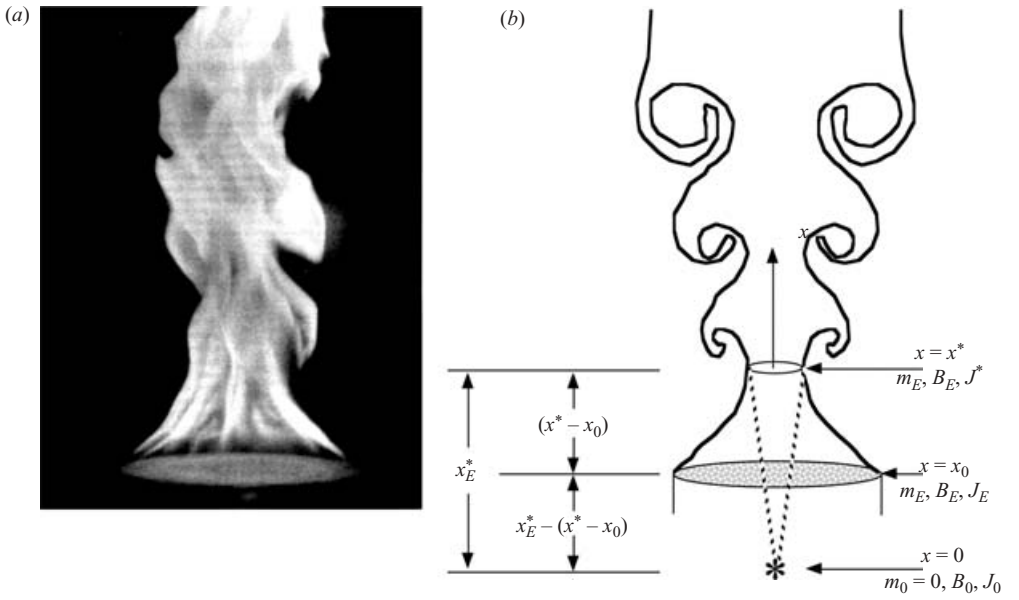

FIGURE 4. The virtual origin of buoyant jets with $J_E < J^*$ in (48), showing (*a*) typical flame photograph from Delichatsios (1987) and (*b*) schematic representation. Since J_E is incompatible with m_E and B_E, no entrainment of ambient fluid occurs until buoyancy has increased the momentum flux $J(x)$ from the exit value J_E at x_E to the minimum value J^* at x^* that is compatible with m_E and B_E.

heat will be added over this region. As a result, (49) can be integrated from J_E at x_0 to determine the location x^* at which $J(x)$ has increased to J^* in (48), giving

$$(x^* - x_0) = \frac{1}{2}\left(\frac{I_1 I_4}{I_2 I_3}\right)\frac{(J^{*2} - J_E^2)}{m_E B_E}. \tag{50}$$

With $m(x^*) = m_E$, $B(x^*) = B_E$ and $J(x^*) = J^*$, the flow for $x \geqslant x^*$ corresponds to a pure plume produced by an equivalent point source located upstream of the x^*-plane by the distance x_E^* given by (16), and thus at $x_E = x_E^* - (x^* - x_0)$ upstream of the actual exit plane, as in figure 4. When x is instead used to denote the downstream distance measured from the exit of the actual source, rather than the distance from the ideal point source, then x in $\delta(x)$ and $u_c(x)$ must be replaced by $x + x_E$ where x_E is obtained as above from x_E^* in (16) and $(x^* - x_0)$ in (50) with J^* from (48).

4. Exothermic reacting buoyant jets

The results from §§2 and 3 now allow a solution for exothermically reacting turbulent buoyant jets. Note first that, even in the absence of any buoyancy effects, the reduction in density due to heat release alters the inertia of the flow, and thereby can affect the scaling laws for $\delta(x)$ and $u_c(x)$. Part 1 has shown that, because of the bilinear variation of temperature with mole fraction required by enthalpy conservation, the inertial effects of density changes due to exothermic reaction are equivalent to a reduction in the ambient fluid density to an effective value determined by the peak temperature and overall stoichiometry. The equivalence principle from Part 1 thus allows the scaling laws for $\delta(x)$ and $u_c(x)$ in a non-reacting flow to be properly extended to the corresponding exothermically reacting flow by replacing the

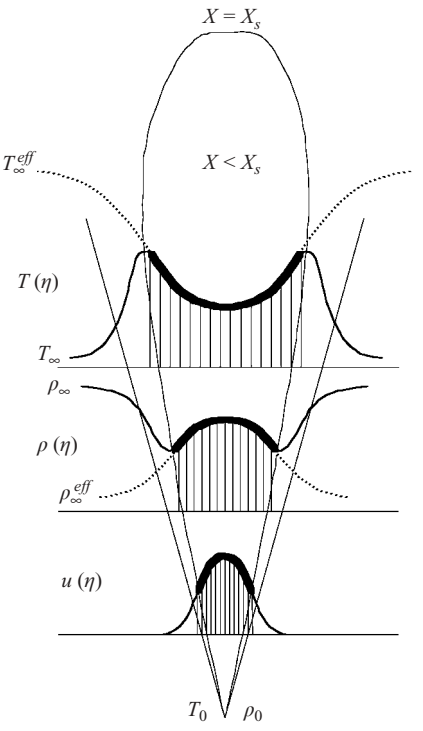

FIGURE 5. Schematic of equivalence principle from Parts 1 and 2, showing implications for mean temperature (top) and density (middle) profiles in an exothermically reacting jet. Solid lines show profiles in exothermic reacting flow; dashed lines show profiles in nonreacting flow produced by simple mixing between the actual source values T_0 and ρ_0 effective ambient values T_∞^{eff} and ρ_∞^{eff}. Heavy line shows resulting agreement for $X > X_S$, where velocity (bottom) is large, ensuring proper accounting for dominant inertial effects of heat release.

ambient density ρ_∞ with ρ_∞^{eff}, where

$$\rho_\infty^{eff} = \rho\left(\frac{T_\infty}{T_\infty^{eff}}\right) \quad \text{with} \quad T_\infty^{eff} \equiv T_0 + \frac{T_s - T_0}{1 - X_s}, \tag{51}$$

with T_0 and T_∞ the source and ambient fluid temperatures, and T_S and X_S the stoichiometric values of the temperature and jet-fluid mole fraction.

This equivalence is shown for the mean temperature, density and velocity profiles in figure 5. As discussed in Parts 1 and 2, where $X > X_S$ (heavy line) the temperature and density profiles in the reacting flow (solid line) are the same as those in a non-reacting flow (dashed line) resulting from simple mixing between the actual source values and the effective ambient values in (51). The equivalence principle developed in Part 1 thus ensures the correct density in those parts of the flow where the velocity is highest, and thereby provides a fundamentally correct accounting for the inertial effects of heat release on the far-field scaling laws for $\delta(x)$ and $u_c(x)$. These outer length and velocity scales in turn determine the entrainment and mixing properties and the resulting flame length in such flows. Parts 1 and 2 have verified that this equivalence principle accurately predicts effects of heat release in both the near- and far-fields of planar and axisymmetric turbulent jets, as well as in planar turbulent mixing layers.

This equivalence allows the results for non-reacting buoyant jet results to be extended to address buoyancy effects due to heat release in exothermically reacting jets and plumes. In such exothermically reacting buoyant jets, the radial profile in (3*b*) of the nominal density-difference $\Delta\rho \equiv \rho_\infty - \rho$ will no longer be self-similar, and this might appear to preclude any integral method for such flows. However as noted above, it is instead the effective density-difference profile $(\Delta\rho)_{eff} \equiv \rho - (\rho_\infty)_{eff}$ that is relevant to momentum conservation in such flows, and this profile remains self-similar. Closely related to this, Chen & Rodi (1980) show that $\delta \sim x$ is a requirement for such self-similarity, and thus is consistent with the present (22*a*). (Note also that localized heat addition, as in the experiments of Bhat & Narasimha (1996) and Agrawal & Prasad (2004), fundamentally precludes self-similarity and thus cannot be addressed by the present method.)

We therefore return to the flow in § 3 issuing from an ideal point source that introduces source values of the momentum flux J_0 and buoyancy flux B_0, as in the previous section, but now the heat released by reaction produces an increase in the buoyancy flux $B(x)$. However, (21) and (22) show that $\delta(x)$ in buoyant jets is independent of the ambient fluid density, and thus remains unchanged when ρ_∞ is replaced by ρ_α^{eff} experimental data confirming the invariance of $\delta(x)$ in jets with heat release is given in Part 1. By contrast, the presence of $B(x)$ in (31) shows that the centreline velocity $u_c(x)$ is affected by buoyancy. In this section, the equation for the buoyancy flux is shown to allow an expression for $B(x)$ in terms of the centreline velocity $u_c(x)$, and on substituting into (31) this is shown to provide a remarkably simple equation for $u_c(x)$ into exothermically reacting turbulent buoyant jets.

4.1. *The buoyancy flux* $B(x)$

When, as is typically the case, the buoyancy is produced by temperature differences, and when variations in the molecular weight and specific heat can be neglected (see Part 1), then the buoyancy flux $B(x)$ in (1*c*) is related to the heat flux $Q(x)$ as

$$\frac{\mathrm{d}B}{\mathrm{d}x} = \left(\frac{g}{c_p T_\infty}\right)\frac{\mathrm{d}Q}{\mathrm{d}x}, \tag{52}$$

where g is the acceleration into gravity, c_p is the specific heat of the stoichiometric reactant mixture, and T_∞ is the ambient temperature. For entrainment-limited mixing and mixing-limited reaction, as typically applies in non-premixed or partially premixed turbulent reacting flows, at any x-location upstream of the flame tip, the local rate of heat release $\mathrm{d}Q(x)/\mathrm{d}x$ is set by the local rate of entrainment $\mathrm{d}m(x)/\mathrm{d}x$ via

$$\frac{\mathrm{d}Q}{\mathrm{d}x} \sim \Delta h_c \frac{\mathrm{d}m}{\mathrm{d}x}, \tag{53}$$

where Δh_c is the enthalpy of combustion per unit mass of fuel. The proportionality in (53) results because the local rate of molecular mixing is about one-third the local rate of entrainment, as has been shown in the jet-limit by Dahm & Dimotakis (1987) and in the plume-limit by Cetegen *et al.* (1984). Thus, the integral equation for $B(x)$ becomes

$$\frac{\mathrm{d}}{\mathrm{d}x}B(x) = \Pi\frac{\mathrm{d}}{\mathrm{d}x}m(x) \tag{54}$$

where

$$\Pi = \left(\frac{g\,\Delta h_c}{3c_p T_\infty}\right). \tag{55}$$

Substituting (6*a*) for the mass flux $m(x)$ in (54), and using $\delta(x)$ from (22*a*), gives

$$\frac{\mathrm{d}}{\mathrm{d}x}B(x) = I_1 c_\delta^2 \Pi \frac{\mathrm{d}}{\mathrm{d}x}(x^2 u_c), \tag{56}$$

which integrates directly to give

$$\left(B(x)/\rho_\infty^{eff}\right) = I_1 c_\delta^2 \Pi \left(x^2 u_c(x) - x_E^2 u_{cE}\right) + \left(B_E/\rho_\infty^{eff}\right). \tag{57}$$

As above, x_E is the x-location of the exit from the virtual origin, so that $B(x_E) = B_E$ and $u_c(x_E) \equiv u_{cE}$.

4.2. *The centreline velocity* $u_c/u^* = f_2(\chi;\Lambda)$

The momentum equation in (31) may be multiplied by x2 and rearranged to give

$$\frac{\mathrm{d}}{\mathrm{d}x}(x u_c)^3 = 3\sigma x \left(B(x)/\rho_\infty^{eff}\right), \tag{58}$$

where from (41)

$$\sigma = \tfrac{2}{3}(c_u)_p^3. \tag{59}$$

Substituting the result in (57) for the buoyancy flux gives

$$\frac{\mathrm{d}}{\mathrm{d}x}(x u_c)^3 = 3\sigma I_1 c_\delta^2 \Pi x^3 u_c - x\left[3\sigma I_1 c_\delta^2 \Pi x_E^2 u_{cE} - 3\sigma\left(B_E/\rho_\infty^{eff}\right)\right]. \tag{60}$$

In the dimensionless centreline velocity and downstream coordinate in (32) this becomes

$$\frac{\mathrm{d}}{\mathrm{d}\chi}(\chi f_2)^3 = \Lambda \chi^3 f_2 - \chi\left[\Lambda \chi_E^2 f_2(\chi_E) - 2(c_u)_p^3\right], \tag{61}$$

where

$$\Lambda \equiv 2 I_1 c_\delta^2 (c_u)_p^3 \frac{\left(J_0/\rho_\infty^{eff}\right)^{5/4}}{\left(B_0/\rho_\infty^{eff}\right)^{3/2}} \Pi, \tag{62}$$

and where J_0 is obtained from (46) and $B_0 = B_E$ as noted in § 3.4. This may be put in a more compact form by defining

$$w \equiv (\chi f_2)^3, \tag{63a}$$

$$b \equiv \Lambda \chi_E^2 f_2(\chi_E) - 2(c_u)_p^3, \tag{63b}$$

for which (61) becomes

$$\frac{\mathrm{d}w}{\mathrm{d}\chi} = \Lambda \chi^2 w^{1/3} - b\chi. \tag{64}$$

The result in (64) is a single equation for $f_2(\xi;\Lambda)$ that can be numerically integrated from initial values χ_E and w_E determined by the exit mass, momentum and buoyancy fluxes, m_E, J_E and B_E, to determine the centreline velocity $u_c(x;\Lambda)$ in exothermic reacting turbulent buoyant jets.

4.3. *Application to cases with* $B_E < 0$

Before returning to (64), we show here that it applies even in certain cases for which $B_E < 0$, as can occur in many practical applications. Specifically, when the exit buoyancy flux B_E is sufficiently small in comparison with the total added buoyancy flux $(B_L - B_E)$ from heat release between the exit and the flame tip (here the subscript

L denotes quantities at the flame tip location $x = L$; see § 5), then $B(x)$ is dominated by the heat release and the effect of B_E becomes negligible. From (54), this is the case whenever the fractional increase in buoyancy flux due to heat release is sufficiently large, namely when

$$\frac{(B_L - B_E)}{|B_E|} = \left(\Pi \frac{m_E}{|B_E|}\right)\left(\frac{m_L}{m_E} - 1\right) \gg 1.$$

From § 5, it can be shown that

$$\frac{m_L}{m_E} = \frac{20}{\sqrt{\pi}} I_1 c_\delta^2 (c_u)_j (1 + \varphi),$$

where φ is the stoichiometric ambient-to-exit fluid mass ratio. Thus, B_E is negligible when

$$\left(\Pi \frac{m_E}{|B_E|}\right)\left(\frac{20}{\sqrt{\pi}} I_1 c_\delta^2 (c_u)_j (1 + \varphi) - 1\right) \gg 1.$$

Since $\varphi \gg 1$ for hydrocarbon fuels issuing into air, this requirement is clearly satisfied in most practical circumstances. In such cases, B_E could be set to zero; however, to avoid $l^* \to \infty$ and $u^* \to 0$ in (17*a*) and (17*b*) and $\Lambda \to \infty$ in (62) with (46), B_E can equally well be set to any negligible positive value; e.g. $|B_E|$ as done herein.

4.4. *Practical implementation*

For given values of the exit mass, momentum and buoyancy fluxes, m_E, J_E and B_E in (2*a*)–2(*c*), the result in (64) can be readily applied as follows to determine the centreline velocity $u_c(x; \Lambda)$, and thus with $\delta(x) = c_\delta x$ in (22*a*) to thereby determine the resulting mass, momentum and buoyancy fluxes, $m(x)$, $J(x)$ and $B(x)$ via (6*a*)–(6*c*), as well as quantities such as the entrainment and mixing rate $\mathrm{d}m/\mathrm{d}x$:

(i) For exothermic reacting cases, the effective ambient fluid density ρ_∞^{eff} is first computed via (51) and ρ_∞ is everywhere replaced by ρ_∞^{eff}; for non-reacting cases the ambient fluid density ρ_∞ applies throughout.

(ii) If $J_E > J^*$ in (48), then χ_E is obtained from (47), which applies between the ideal point source and the exit of the actual finite-area source, namely $0 \leqslant x \leqslant x_E$, since even in exothermic cases no heat release occurs before the flow issues from the actual source. From χ_E the momentum flux J_0 of the equivalent ideal point source is obtained from (46). The buoyancy flux B_0 of the equivalent point source is then $B_0 = B_E$, since no heat release occurs in the range $0 \leqslant x \leqslant x_E$. From J_0 and B_0, l^* and u^* are obtained via (17*a*) and (17*b*).

If $J_E < J^*$, then $x_E = x_E^* - (x^* - x_0)$ where x_E^* is from (16) and $(x^* - x_0)$ is from (50) with J^* from (48). In such cases, $B_0 = B_E$ but $J_0 = 0$, and thus the flow for $x \geqslant x^*$ is a reacting plume. To avoid $l^* = 0$ and $u^* = \infty$, J_0 can be set to any sufficiently small value so that $\chi_E = x_E/l^*$ is in the plume limit $\chi_E > 10$. From J_0 and B_0, l^* and u^* are obtained via (17*a*) and (17*b*).

(iii) From χ_E and the constants $(c_\mu)_j$ and $(c_\mu)_p$ given in (8*b*) and (13*b*), the corresponding $f_2(\chi_E)$ is obtained from (42), which applies in the range $0 \leqslant x \leqslant x_E$ since no heat release occurs before the flow issues from the actual source; u_{cE} is then obtained from u^* via (18*b*).

(iv) The initial value w_E is obtained from χ_E and $f_2(\chi_E)$ via (63*a*).

(v) Λ is obtained from (62) with I_1 given by (5*a*), c_δ by (22*b*), and Π from (55) with T_∞ the actual ambient fluid temperature.

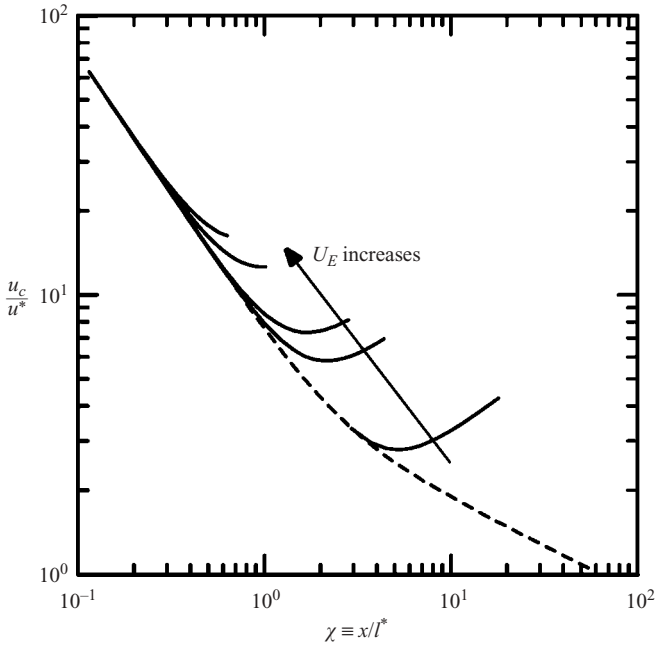

FIGURE 6. Centreline velocity $u_c(x)$ in exothermic reacting turbulent buoyant jets from integration of (64), showing the effect of increasing the source exit velocity U_E with fixed exit diameter ($d_E = 1\,\text{cm}$) for a C_3H_8 jet issuing into air. Exit values m_E, J_E and B_E in (2*a*)–(2*c*) differ for each U_E values, leading to different initial conditions χ_E in (47). Results are shown for five different exit velocities ($U_E = 1, 5, 10, 50, 100\,\text{m s}^{-1}$) (solid lines) from jet exit to flame tip, with non-reacting curve (dashed line) from figure 2 shown for comparison. Velocity initially decays for all cases, but for strongly buoyant cases subsequently increases as buoyancy accelerates fluid.

(vi) Equation (64) is integrated forward from the initial condition (χ_E, w_E); the integration continues until the flame tip criterion in (73) is reached (see § 5), with κ from (77).

(vii) For χ beyond the flame tip, the integration can be continued, but no further heat release occurs, and thus, past this point, Λ in (64) is set to zero with the result that $B(x)$ remains constant from there on; from Part 1, past the flame tip, the effective density is determined by the lean branch of $T(X)$, and thus ρ_0 is replaced by ρ_0^{eff} and ρ_∞^{eff} is replaced by ρ_∞.

(viii) The resulting $w(\chi)$ then gives the centreline velocity $u_c(x)$ via (32*a*) and (32*b*); the local flow width $\delta(x)$ is obtained trivially from (22*a*) and (22*b*).

(ix) The resulting $u_c(x)$ and $\delta(x)$ can then be used to obtain the mass flux $m(x)$ via (6*a*), the momentum flux $J(x)$ via (6*b*), and the buoyancy flux $B(x)$ via (6*c*), with the density ρ_∞ replaced by ρ_∞^{eff} from (51).

4.5. *Sample results*

Figures 6–8 show example results obtained from this integral method for various parametric effects on the centreline velocity $u_c(x)$ in exothermic reacting buoyant jets. Figure 6 gives results showing the effect of the source exit velocity U_E in (2*a*)–(2*c*), figure 7 shows the effect of A_E in (2*a*)–(2*c*) via the exit diameter d_E, and figure 8 shows the effect of the fuel type. Each curve in these figures shows results from the exit location x_E to the flame tip corresponding to the criterion in (73) below. The dashed

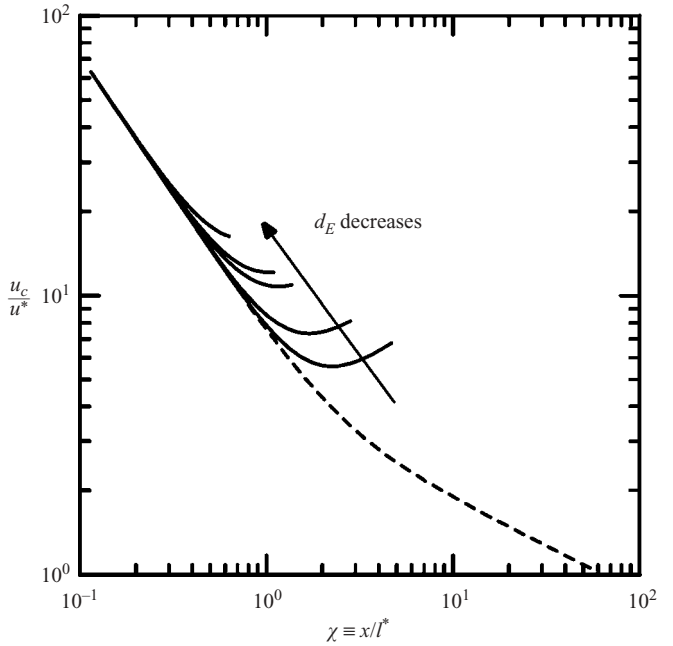

FIGURE 7. Similar to figure 6, but showing the effect of decreasing the exit diameter d_E with fixed exit velocity ($U_E = 10\,\mathrm{m\,s^{-1}}$) for a C_3H_8 jet issuing into air. Exit values m_E, J_E and B_E in (2*a*)–(2*c*) differ for each d_E value, leading to different initial conditions χ_E in (47). Results are shown for five different exit diameters ($d_E = 50, 10, 5, 1, 0.5, 0.1$ mm) (solid lines) from jet exit to flame tip, with non-reacting curve (dashed line) from figure 2 shown for comparison.

curve in each case is the non-reacting result in (42) for otherwise identical conditions, allowing comparisons with each solid curve to show the effect of heat release. In each case the centreline velocity initially follows the non-reacting curve, and then as the buoyancy flux $B(x)$ increases significantly beyond its source value B_E due to combustion heat release, the solid curves depart from the non-reacting curve. In most cases shown, the centreline velocity reaches a minimum at some downstream location, beyond which it increases as the added buoyancy due to heat release accelerates the fluid more rapidly than the increase in $\delta(x)$ can spread the added momentum across the lateral direction.

In particular, figure 6 shows results for a propane jet issuing into air through a constant 1 cm exit diameter dE for exit velocities U_E ranging from $1\,\mathrm{m\,s^{-1}}$ to $100\,\mathrm{m\,s^{-1}}$. The former produces low exit values m_E, J_E and B_E that correspond to initial values χ_E as large as 3, and thus the flow is already between the jet-like and plume-like limits even at the exit. By contrast, for $U_E = 100\,\mathrm{m\,s^{-1}}$ the comparatively high exit values m_E, J_E and B_E produce initial values χ_E as small as 0.02, for which the flow is initially jet-like. For all χ_E values, the centreline velocity decrease initially follows the non-reacting form given by the dashed line, until the added buoyancy flux due to heat release becomes significant relative to the initial value B_E. At this point, the rate of velocity decay becomes slower than in the non-reacting jet. Each curve continues to the χ value corresponding to the flame tip location χ_L as determined in § 5. For cases that extend to sufficiently large χ, the centreline velocity increases with increasing downstream distance χ owing to the effect of the added buoyancy.

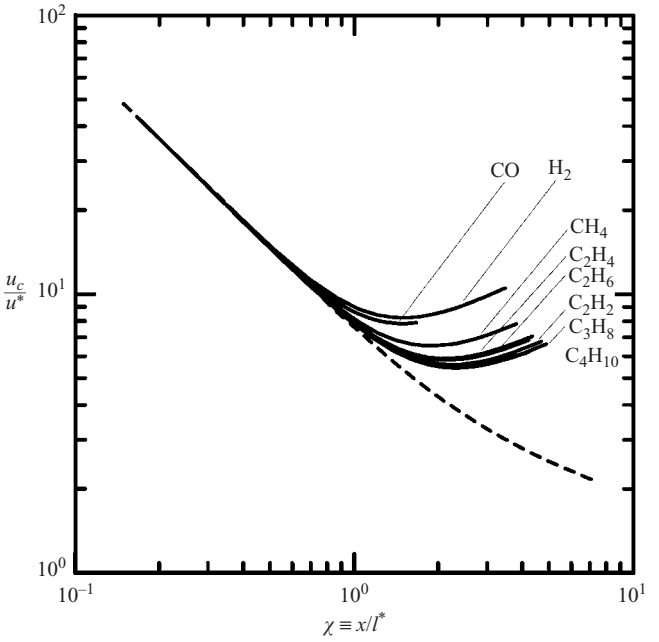

FIGURE 8. Similar to figures 6 and 7, but showing the effect of fuel type for various fuels issuing into air with fixed exit diameter and exit velocity ($d_E = 5\,\text{cm}$, $U_E = 10\,\text{m s}^{-1}$). Results are shown for eight fuels (solid lines) from jet exit to flame tip, with non-reacting curve from figure 2 (dashed line) shwon for comparison. Exit values m_E, J_E and $|B_E|$ in (2*a*)–(2*c*) change for each curve owing to differing exit densities ρ_E, leading to different χ_E values in (47). Heat release parameter Π in (55) also varies with fuel type, as does stoichiometric mass ratio φ in (72), leading to differences in flame lengths.

Figure 7 shows similar results for propane–air flames, but here U_E is kept constant at 10 m s^{-1} and the d_E is varied from 0.1 mm to 50 mm. The smallest exit diameter produces exit values m_E, J_E and B_E that correspond to a small initial value χ_E, while for $d_E = 50\,\text{mm}$ the resulting m_E, J_E and B_E produce a comparatively large χ_E. Each curve again extends to the corresponding flame tip value χ_L. Comparing with the previous figure, it is apparent that the only difference between figures 6 and 7 is in the initial value χ_E for each case, since the fuel type is the same, and thus the curves fall onto a continuous family parameterized by χ_E.

In figure 8, the exit diameter and velocity are held constant, and the fuel type is varied. Thus, each curve begins at the same initial value χ_E, and extends to the flame tip value χ_L, which depends on the stoichiometric fuel–air mass ratio φ as shown in § 5. The fuel heating value Π in (55) also differs among these fuels, and thus so does Λ in (62) and (64). The combined effects of Λ and φ lead to the differences in the centreline velocity decay seen in figure 8. Note that, with the exception of hydrogen (H_2) and carbon monoxide (CO), the differences among the remaining fuels are fairly small. It is for this reason that most previous studies of buoyancy effects in jet flames have been based on correlations for 'typical' fuels. However, the present approach requires no such restriction or empiricism, and applies equally from momentum dominated jet flames to purely buoyant pool fires.

Figures 9–11 show results from the present integral method for the mass flux $m(x)$, momentum flux $J(x)$, and buoyancy flux $B(x)$ from (6*a*)–(6*c*) along the length of a

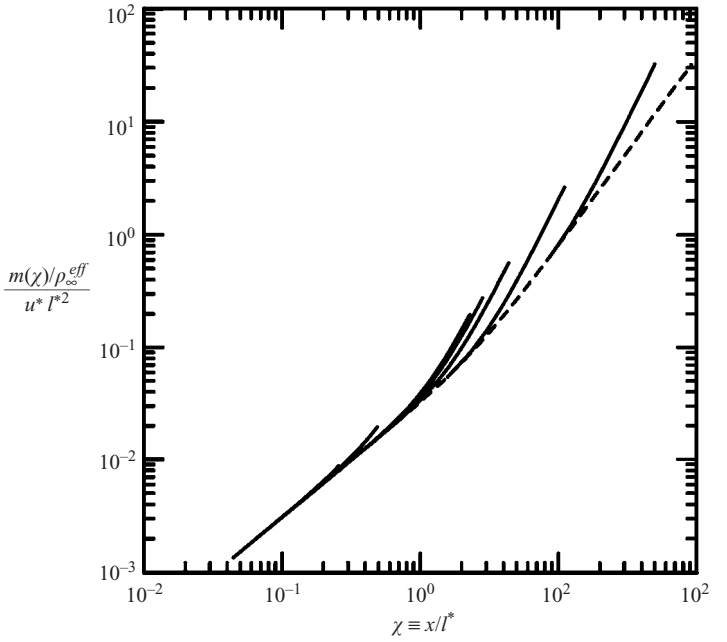

FIGURE 9. Mass flux $m(x)$ in (6*a*) for exothermic reacting turbulent buoyant jets of propane issuing into air, obtained from integration of (64). Results are shown from jet exit at χ_E to flame tip at χ_L for seven combinations of exit diameter d_E and exit velocity U_E in table 1. Exit values m_E, J_E and $|B_E|$ in (2*a*)–(2*c*) differ for each curve, leading to different initial values χ_E in (47). Note that mass flux increases as $m(x) \sim x$ in the jet limit $\chi \ll 1$, in accordance with (9), and transitions to $m(x) \sim x^{5/3}$ in the plume limit $\chi \gg 1$, in accordance with (14*a*).

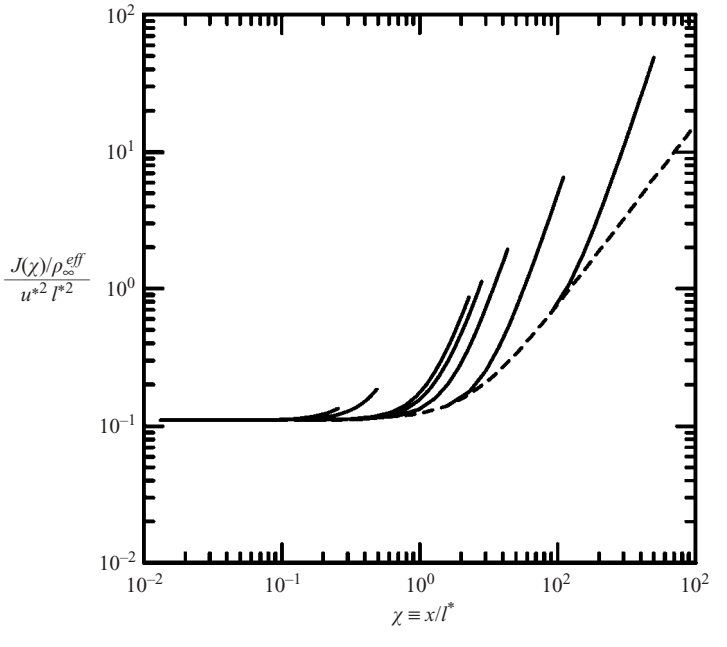

FIGURE 10. Momentum flux $J(x)$ in (6*b*) for the same cases as shown in figure 9. Note that the momentum flux remains constant in the jet limit $\chi \ll 1$, and subsequently increases as $J(x) \sim x^{4/3}$ in the plume limit $\chi \gg 1$ in accordance with (14*b*).

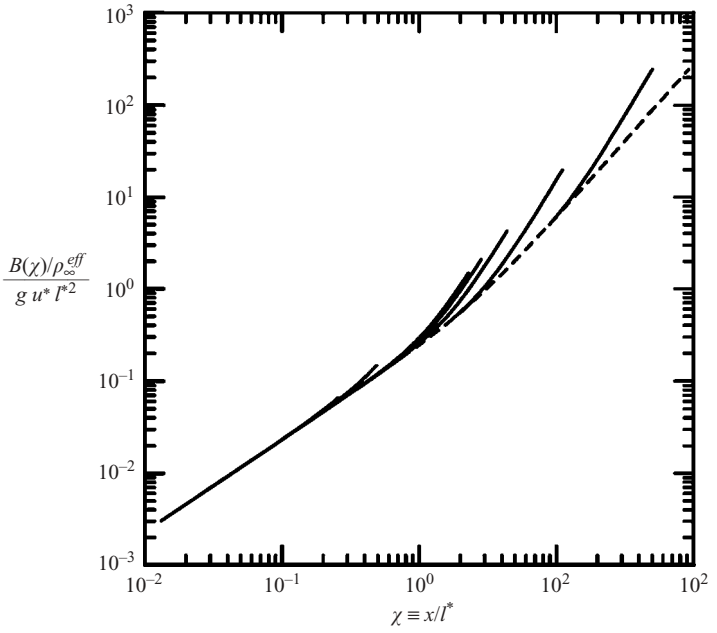

FIGURE 11. Buoyancy flux $B(x)$ in (6c) for the exothermic reacting turbulent buoyant jets in table 1. In accordance with (54) and figure 9, the buoyancy flux increases as $B(x) \sim x$ in the jet limit $\chi \ll 1$, and as $B(x) \sim x^{5/3}$ in the plume limit $\chi \gg 1$.

U_E (m s^{-1})	d_E (mm)	x_E/l^*	u_{cE}/u^*
100	1	0.006	1220
100	5	0.013	546
10	5	0.132	54.6
10	10	0.187	38.6
5	10	0.378	19.2
1	5	1.574	5.1
0.8	10	8.936	2.0

TABLE 1. Exit velocity U_E and exit diameter d_E for exothermic reacting turbulent buoyant jets of propane issuing into air shown in figures 8–10. Resulting exit values m_E, J_E and B_E in (2a)–(2c) produce different initial values x_E from (47) and corresponding u_{cE} values from (42), as well as different values of the Morton length and velocity scales l^* and u^* from (17a) and (17b).

reacting propane jet issuing into air for each combination of exit velocity U_E and exit diameter d_E given in table 1. The corresponding exit conditions x_E and u_{cE} from (47) and (42), normalized by the Morton length and velocity scales l^* and u^* from (17a) and (17b) with (46), are also shown in table 1. Each curve in these figures shows results from the exit location x_E to the flame tip corresponding to the criterion in (72). The curves each start at their respective χ_E value on the dashed line obtained from the non-reacting result in figure 3, and depart in a manner that depends on their respective Λ value.

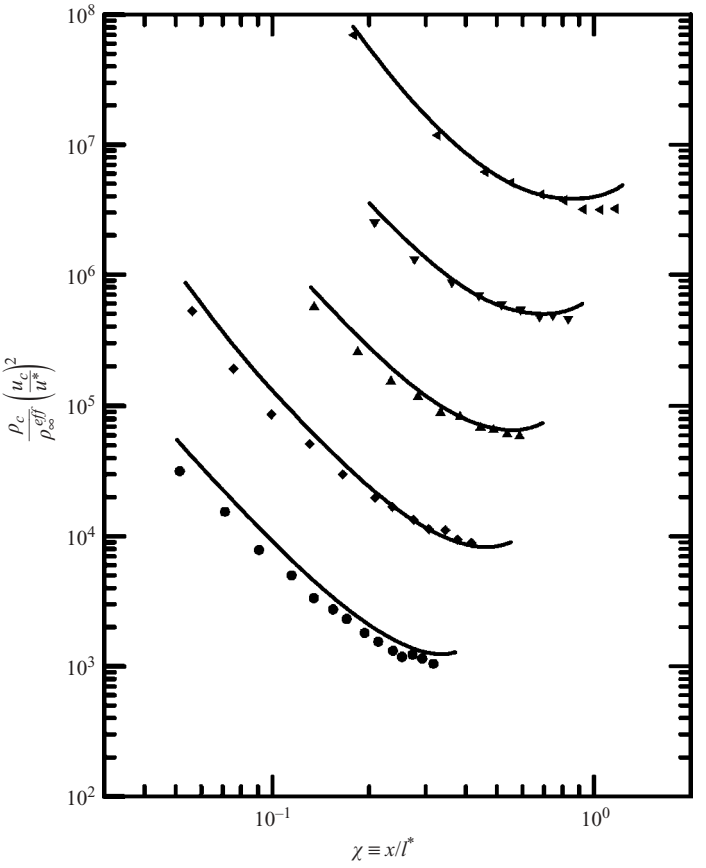

FIGURE 12. Centreline dynamic pressure $\rho_c u_c^2$ in exothermic reacting turbulent buoyant jets, comparing experimentally measured values of Becker & Yamazaki (1978) (symbols) with corresponding results from present integral method (lines). Experimental conditions for each case are given in table 2. For clarity, each case has been shifted vertically by one decade.

U_E (m s^{-1})	d_E (mm)
17.6	4.6
27.3	4.6
42.2	4.6
59.6	4.6
79.0	2.5

TABLE 2. Exit velocity U_E and exit diameter d_E for exothermic reacting turbulent buoyant jets of propane issuing into air from Becker & Yamazaki (1978), shown in figures 11–13 and listed in the same order as they appear in the figures.

Figures 12–14 provide comparisons with various quantities – obtained from experimentally measured values in the propane–air flames of Becker & Yamazaki (1978), for which the corresponding exit velocity U_E and exit diameter d_E are given in table 2. In each case, results obtained from the present integral method for the same exit conditions, shown by the solid curves, are seen to compare well with the corresponding

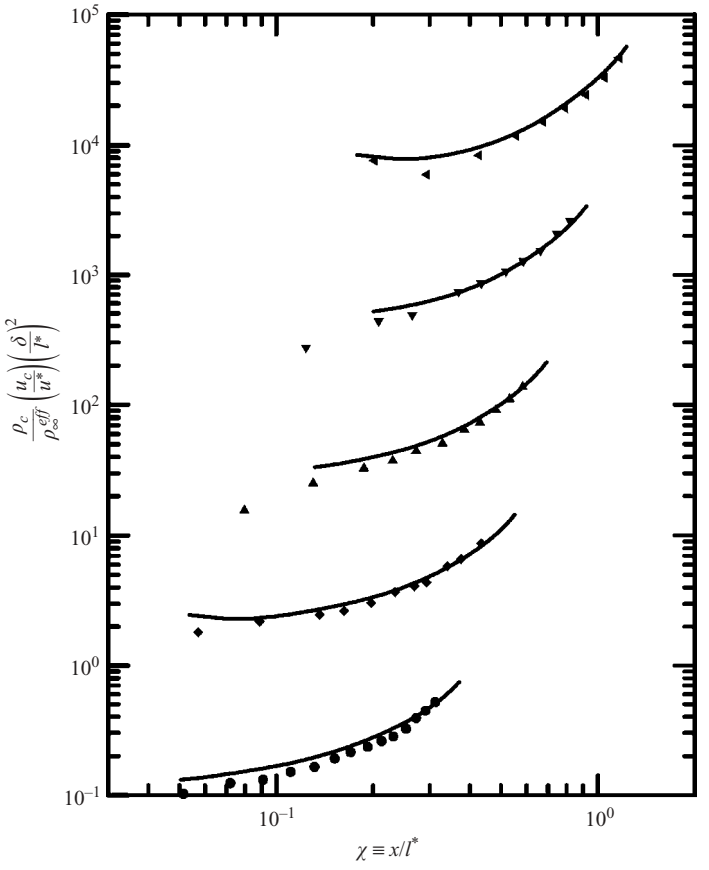

FIGURE 13. Mass flux scaling $\rho_c u_c \delta^2$ in exothermic reacting turbulent buoyant jets, comparing results obtained from measured data of Becker & Yamazaki (1978) (symbols) with corresponding results from present integral method (lines). Experimental conditions for each case are given in table 2. For clarity, each case has been shifted vertically by one decade.

measured values. Each of the curves is obtained as outlined above, with no adjustable parameters to force agreement with the measured values. Each curve continues up to the flame tip obtained from the criterion in (73) in the following section.

5. Flame length of exothermic reacting buoyant jets

The flame tip occurs at the downstream location where the centreline value of the source–fluid mixture fraction $\zeta_c(x)$ reaches the stoichiometric value ζ_s, as shown below.

5.1. *The flame tip criterion*

Since the mixture fraction is a conserved scalar, the total scalar flux integral

$$m_\zeta = \int_0^\infty \overline{\rho u \zeta}(x, r) 2\pi r \, \mathrm{d}r \tag{65}$$

is an invariant of the scalar field. In a manner similar to (6*a*), this can be written as

$$m_\zeta(x) \approx I_4 \rho_\infty^{eff} \zeta_c(x) u_c(x) \delta^2(x), \tag{66}$$

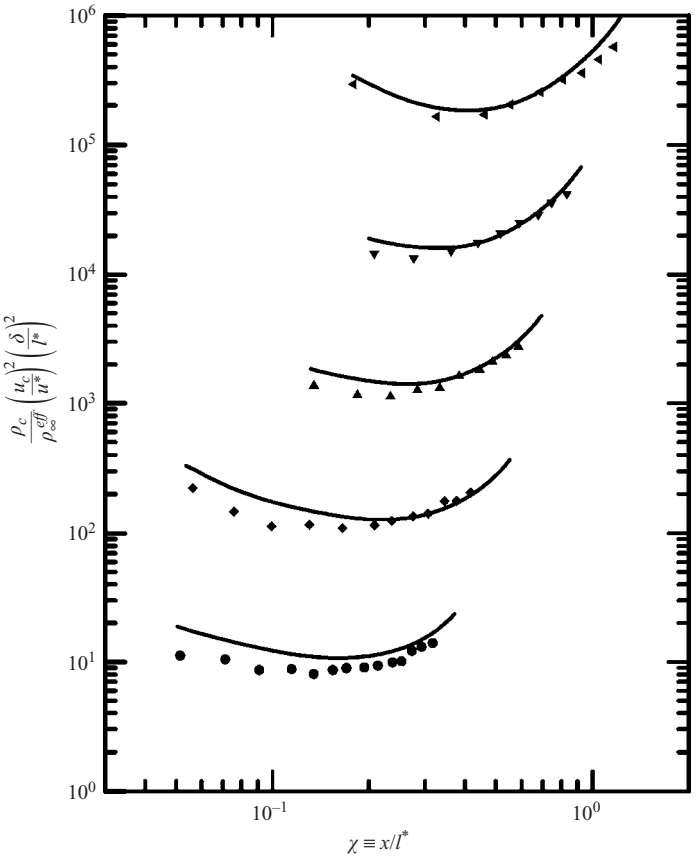

FIGURE 14. Momentum flux scaling $\rho_c u_c^2 \delta^2$ in exothermic reacting turbulent buoyant jets, comparing results obtained from measured data of Becker & Yamazaki (1978) (symbols) and corresponding results from present integral method (lines). Experimental conditions for each case are given in table 2. For clarity, each case has been shifted vertically by one decade.

where we have additionally made use of

$$\frac{\bar{\zeta}(x,r)}{\zeta_c(x)} = h(\eta), \tag{67}$$

with $h(\eta)$ as given in (3*b*). This gives the mean centreline mixture fraction as

$$\zeta_c(x) = \frac{1}{I_4}\frac{m_\zeta}{\rho_\infty^{eff} u_c(x)\delta^2(x)}, \tag{68}$$

and defining the mixture fraction ζ_E at the exit of the actual source as

$$\zeta_E = \frac{m_\zeta}{m_E} \tag{69}$$

gives

$$\frac{\zeta_c}{\zeta_E} = \frac{1}{I_4}\frac{m_E}{\rho_\infty^{eff} u_c(x)\delta^2(x)}. \tag{70}$$

Substituting from (22a, b) and (32a, b), with (17a, b), then gives

$$\frac{\zeta_c}{\zeta_E} = \frac{1}{I_4 c_\delta^2} \left[\frac{\left(m_E/\rho_\infty^{eff}\right)\left(B_E/\rho_\infty^{eff}\right)^{1/2}}{\left(J_0/\rho_\infty^{eff}\right)^{5/4}} \right] \frac{1}{\chi^2 f_2(\chi)}, \tag{71}$$

where J_0 is as discussed in § 4.4. We will use φ to denote the stoichiometric ambient-to-exit fluid mass ratio; thus for example, for a source issuing pure methane (CH_4) into air, the stoichiometric mass ratio is $\varphi = 17.2$. In terms of the source–fluid mixture fraction, the stoichiometric requirement is

$$\frac{\zeta_s}{\zeta_E} = \frac{1}{1+\varphi}, \tag{72}$$

where ζ_s is the stoichiometric mixture fraction. The flame tip occurs at $x = L$ where the centreline mixture fraction $\zeta_c(x)$ reaches a value proportional to the stoichiometric requirement, namely $\zeta_c(L) = \kappa \zeta_s$. Substituting in (71) gives the criterion for the flame length L as

$$\chi_L^2 f_2(\chi_L) = \frac{1}{I_4 c_\delta^2 \kappa} \left[\frac{\left(m_E/\rho_\infty^{eff}\right)\left(B_E/\rho_\infty^{eff}\right)^{1/2}}{\left(J_0/\rho_\infty^{eff}\right)^{5/4}} \right] (1+\varphi). \tag{73}$$

The integration of (64) thus continues until the left-hand side of (73) reaches the value on the right, at which point the flame tip location $\chi_L \equiv L/l^*$ has been reached. It is in this manner that the stoichiometric fuel–air mass ratio φ enters in setting the flame tip location. The value of κ on the right-hand side of (73) can be obtained from the jet-limit flame length scaling in Part 1, namely

$$L/d^+ = 10(1+\varphi), \tag{74}$$

by taking the limit $\chi \to 0$ in (73), using (36) and (38) with (8b), together with (18c) and (17a), which give

$$(L/d^+) = \frac{\sqrt{\pi}/2}{I_4 c_\delta^2 (c_u)_j \kappa}(1+\varphi), \tag{75}$$

where

$$d^+ = \left(\rho_\infty/\rho_\infty^{eff}\right)^{1/2} d^* \tag{76}$$

and d^* is defined in (11). Thus,

$$\kappa = \frac{\sqrt{\pi}}{20 I_4 c_\delta^2 (c_u)_j}, \tag{77}$$

and from values above for the various constants (77) gives $\kappa \approx 0.69$. With this value of κ, (73) gives the mean luminous flame tip location, since the factor of 10 in (74) is from a compilation of luminous flame length data (Dahm & Dimotakis 1987); other values of this factor correspond to other definitions of the flame length. Flame length fluctuations ΔL around the mean length L in (73) are due to mixture fraction fluctuations produced by the local large-scale structure of the flow, and thus $\Delta L \approx \delta(L)$ (Dahm & Dimotakis 1987; Mungal & Hollingsworth 1989) with $\delta(L)$ from (22a) and 22(b).

5.2. *The flame length scaling parameters Ω and Λ*

It is apparent that χ_L depends on the combination of parameters on the right-hand side of (73), as well as the heat release parameter Λ that appears in (64) for $f_2(\chi)$,

and thus

$$\chi_L = F\left\{\left[\frac{\left(m_E/\rho_\infty^{eff}\right)\left(B_E/\rho_\infty^{eff}\right)^{1/2}}{\left(J_0/\rho_\infty^{eff}\right)^{5/4}}\right](1+\varphi);\Lambda\right\}. \tag{78}$$

From (18*c*) together with l^* from (17*a*), d^+ from (75) and d^* from (11), the left-hand side of (78) can be expressed in terms of the jet-limit flame length scaling in (74) as

$$\frac{L}{d^+(1+\varphi)} = G\{\Omega;\Lambda\}, \tag{79a}$$

$$\Omega = \left[\frac{\left(J_0/\rho_\infty^{eff}\right)^5}{\left(m_E/\rho_\infty^{eff}\right)^4\left(B_E/\rho_\infty^{eff}\right)^2}\right](1+\varphi)^{-4}. \tag{79b}$$

The flame length scaling in (79) differs from that of Blake & McDonald (1995) and Blake & Cote (1999), and also from the results of Delichatsios (1993). The latter is based on dimensional arguments and scaling considertions in terms of a 'fire Froude number' to correlate flame lengths from the momentum-dominated to the buoyancy-dominated regime. In the present result, Ω and Λ can be seen to be the two parameters that properly determine the effects of buoyancy on the flame. As shown above, these parameters result directly from the governing equations, and differ from the buoyancy parameter ξ obtained heuristically by Becker & Yamazaki (1969) or from the fire Froude number of Delichatsios (1993). Note that the parameter Ω is independent of any heat release, and characterizes the extent to which buoyancy introduced at the source increases the total momentum of the flow over the downstream distance required to entrain and mix the required mass of ambient fluid demanded by the stoichiometric ratio φ. The parameter Λ gives the buoyancy effect due to exothermicity; in conjunction with the former, it determines the additional momentum increase that results from buoyancy created by the density reductions due to heat released within the flow over the downstream distance required to entrain and mix the stoichiometric mass of ambient fluid.

Buoyancy-free flames thus correspond to the simultaneous limit $\Omega \to \infty$ and $\Lambda \to 0$, in which the flame length in (79*a*) must follow the jet-limit scaling in (74), namely $G\{\Omega;\Lambda\} \equiv 10$. Even without any heat release, if m_E, J_E, B_E, ρ_∞^{eff} and φ are such that Ω is sufficiently small then buoyancy will cause the flame length to depart from this jet-limit scaling. Results in the following section show that, for Λ values typical of most combustion situations, this occurs at about $\Omega \approx 10^6$. For Ω values substantially smaller than this, in the $\Lambda \to 0$ limit the flame length can be shown from (14*a*), (69) and (71) to scale as

$$\frac{L}{d^+(1+\varphi)} \sim \Omega^{1/10}. \tag{80}$$

Results in the following section confirm this scaling, and show that it is largely independent of the heat release parameter Λ for the fuel types in table 3 and the range of exit conditions considered there.

5.3. *Comparisons with measured flame lengths*

Figure 15 compares measured values for flame lengths of exothermic reacting turbulent buoyant jet flames over a wide range of conditions, shown in table 3, with corresponding results obtained with the present integral method. The flame lengths are shown in the form of (79), from which it is apparent that the Ω values for these flames span from deep within the buoyancy-dominated plume limit, where $G\{\Omega\} \sim \Omega^{1/10}$,

Reference	Symbol	Fuel	U_E (m s^{-1})	d_E (mm)
Becker & Liang (1978)	●	CH_4	23.8	4.6
		CH_4	32.5	4.6
		CH_4	48.5	4.6
		CH_4	75.6	4.6
		CH_4	88.5	4.6
		CH_4	115	2.5
		CH_4	124	2.5
		CH_4	173	2.5
		CH_4	187	2.5
		CH_4	201	0.7
		CH_4	132	0.7
Muñiz & Mungal (2001)	+	$0.4\ CH_4 + 0.6\ N_2$	36	4.6
		$0.4\ CH_4 + 0.6\ N_2$	134	4.6
Hawthorne, Weddell & Hottel (1949)	◆	CO	17.8	6.4
Hawthorne *et al.* (1949)	▶	H_2	65.6	4.8
Becker & Yamazaki (1987)	▲	C_3H_8	3.5	4.6
		C_3H_8	7.8	4.6
		C_3H_8	17.6	4.6
		C_3H_8	27.3	4.6
		C_3H_8	42.2	4.6
		C_3H_8	59.6	4.6
		C_3H_8	79.0	2.5
Hawthorne *et al.* (1949)	◀	C_2H_2	23.2	3.2
		C_2H_2	31.8	3.2
Wohl, Gazley & Kapp (1949)	■	C_4H_{10}	0.91	10
		C_4H_{10}	1.24	10
		C_4H_{10}	1.90	10

TABLE 3. Fuel type, exit velocity U_E and exit diameter d_E for exothermic reacting turbulent buoyant jets issuing into air in figure 14, listed in same order as they appear in the figure.

to the momentum-dominated jet limit, where $G\{\Omega;\Lambda\} \equiv 10$. The plume-limit scaling is seen to apply for $\Omega < 10^4$, and the jet-limit scaling applies for $\Omega \geqslant 10^6$. The effect of the heat release parameter Λ introduces comparatively small differences among the various curves in figure 15, but the effect of Ω is seen to be far more significant, at least for the conditions reflected in table 3. In each case, it is apparent that the flame lengths obtained from the present integral method compare well with the experimentally measured values. This provides further support for the validity both of the equivalence principle from Parts 1 and 2, and for the present integral method for addressing buoyancy effects in exothermically reacting buoyant jet flames.

6. Concluding remarks

Although computational simulations are increasingly being used to predict the characteristics of exothermic reacting turbulent shear flows for combustion applications, in practice, simple scaling laws are far more widely used to obtain estimates of the resulting integral properties, such as the entrainment and mixing rates, as well as the flame length and other quantities that are of key practical interest. While there are fundamentally-based scaling laws for the integral properties of non-reacting shear flows, at present scaling laws for exothermic reacting shear flows are based either

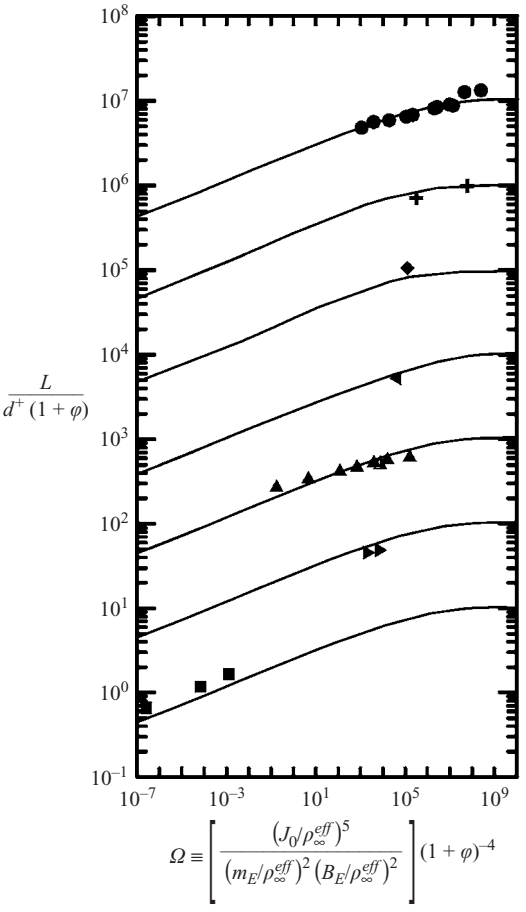

FIGURE 15. Comparison of measured buoyant jet flame lengths (symbols) in table 3 with results from the present integral method (lines), shown in the form of (78). Non-buoyant flames showing the jet-limit scaling in (74) require $\Omega \geqslant 10^6$. Buoyancy-dominated flames show the $\Omega^{1/10}$ plume-limit scaling obtained for $\Lambda = 0$ in (80), even for Λ values corresponding to all cases in table 3. Symbols are defined in table 3; each data set has been shifted upward by one decade for clarity.

on entirely empirical correlations, or on empirical adjustments to the scaling laws for non-reacting flows. There has been debate as to whether it is even conceptually possible to extend scaling laws from non-reacting flows to exothermically reacting flows without substantial resort to empiricism.

It is apparent that heat release can produce changes in numerous comparatively detailed aspects of shear flows (e.g. Han & Mungal 2001; Muñiz & Mungal 2001), but from a practical perspective these are only important insofar as they contribute to changes in the integral flow properties. The present results, together with those in Parts 1 and 2, comprise a significantly improved understanding of how the heat released in exothermic chemically-reacting turbulent shear flows alters the integral flow properties relative to a corresponding non-reacting flow under otherwise identical conditions. These results also provide fundamentally-based methods that extend the scaling laws for non-reacting flows to account for both the inertial effects and buoyancy effects produced by heat release in the corresponding reacting flow.

Part 1 showed that changes in the inertia of the fluid resulting from the reduced densities produced by heat release in mixing-limited reacting shear flows can be accounted for by a fundamental equivalence principle, in which the ambient density ρ_∞^{eff} is replaced by an effective density ρ_∞^{eff} determined via (51) by the stoichiometric temperature T_s and mole fraction X_s. Part 1 showed that this equivalence accurately predicts the heat release effects in the near and far fields of planar and axisymmetric turbulent jet flames over a wide range of conditions, including the reduced entrainment due to heat release in turbulent jets as well as the effect of heat release on the flame length. The equivalence also accurately predicted the much stronger effect of heat release in the far field of planar jets than in axisymmetric jets, and the much larger increase in near-field length owing to heat release in planar turbulent jets than in axisymmetric jets, in good agreement with observations and measurements. In Part 2, this equivalence principle was further applied to address inertial changes due to heat release on the entrainment and mixing properties of turbulent mixing layers. The resulting scaling laws for exothermic reacting mixing layers accurately predicted the very different effects of heat release that occur in that flow. The equivalence principle, however, only accounts for the inertial effects due to the reduced densities produced by heat release, and does not itself account for buoyancy produced by heat release.

Here, we have gone further to show how this equivalence can be extended to exothermic reacting flows in which large buoyancy forces are present, where the buoyancy flux can increase significantly along the length of the flame. The resulting variation in buoyancy flux can produce important changes in the flow properties and the flame length. The present study has developed an integral method for determining the flame length and combustion properties of exothermically reacting buoyant jet flames. The approach avoids the Morton entrainment hypothesis and thereby removes the ad *hoc* 'entrainment modelling' required in most other integral approaches. Rather than working with an integral equation for the entrainment rate $\mathrm{d}m/\mathrm{d}x$, we have used the momentum flux to develop the equation for the local centreline velocity $u_c(x)$. This has the advantage that the modelling can be done in terms of the local flow width $\delta(x)$, for which dimensional considerations show that $\delta(x) \sim x$ in both the momentum-dominated jet limit and the buoyancy-dominated plume limit. Experimental data further show that the proportionality constant c_δ is identical in both the jet and plume limits and remains constant between these two limits as well (e.g. Papanicolaou & List 1988). Thus, whereas the Morton 'entrainment coefficient' α used in most integral methods varies between these two limits, and therefore must be modelled on an *ad hoc* basis in terms of a local Froude number, c_δ in the present method is invariant between these limits and can be represented by a constant value without any further modelling. In effect, the 'entrainment modelling' that is required in traditional integral approaches has been replaced in the present method by the observed constant value of c_δ.

For non-reacting buoyant jets, this new integral approach gives an exact solution for $u_c(x)$ that provides excellent agreement with experimental data, as well as an expression for the virtual origin. In exothermically reacting buoyant jets, the constant c_δ value in the integral equation for the buoyancy flux gives an expression for $B(x)$ in terms of the centreline velocity, and provides a simple integral equation for $u_c(x)$ that can be readily solved for arbitrary exit conditions. The resulting $u_c(x)$ determines the local mass flux $m(x)$, the momentum flux $J(x)$ and the buoyancy flux $B(x)$ throughout the flow, as well as the centreline mixture fraction $\zeta_c(x)$ and the flame length L. Comparisons with data for the centreline velocity and flame length in buoyant jet flames have shown excellent agreement over a wide range of flame

conditions, and provides the parameters Ω and Λ that properly characterize the extent to which buoyancy effects are significant throughout the flame.

Collectively, these results have shown that, when the inertial effects of the reduced densities due to heat release have been properly accounted for via the equivalence principle of Parts 1 and 2, then even the effects of buoyancy produced by heat release can be directly obtained from the scaling laws for buoyancy in the corresponding non-reacting flow under otherwise identical conditions. In other words, the essential fundamental change produced in the flow due to heat release is the inertial change resulting from the reduced density. Once this inertial effect has been accounted for by the fundamental equivalence principle in Parts 1 and 2, then secondary effects of heat release, including buoyancy effects, follow naturally from the scaling laws that govern the non-reacting flow. In this manner, the equivalence principle allows scaling laws for exothermic reacting flows to be directly obtained from the scaling laws for non-reacting flows.

The resulting understanding of how heat release effects are properly accounted for in extending scaling laws for non-reacting flows to exothermic reacting flows allows the large body of existing results from non-reacting shear flows to be applied in combustion science. These include such important practical applications such as the sooting and emissions properties of buoyant flares in the oil and gas industry (e.g. Johnson, Spangelo & Kostiuk 2001). The equivalence principle and the integral method for buoyancy effects presented here can be extended to address crossflow effects on the entrainment and mixing properties of such flares, which would provide scaling laws for flame lengths and emissions properties (e.g. Johnson & Kostiuk 2000, 2002). The same applies to exothermically reacting jets in crossflow (e.g. Karagozian 1986, Nguyen & Karagozian 1992), as well as to heat release and buoyancy effects in vertical enclosures and compartment fires (e.g. Abib & Jaluria 1995; Mercier & Jaluria 1999), where effects of exothermicity on the resulting entrainment and mixing properties can, in principle, be understood within the context of the equivalence principle and the present integral method.

F.J.D. acknowledges financial support by G.M. Faeth at the University of Michigan. Mr Hao Lu provided useful comments on the results provided in this paper. W.J.A.D. acknowledges support, in part, by the National Aeronautics & Space Administration (NASA) Constellation University Institutes Project (CUIP) Space Vehicle Technology Institute (SVTI) under Grant no. NCC3-989, with Claudia Meyer as the project manager. Mr Zachary Nagel provided useful comments on a draft of this paper.

REFERENCES

Abib, A. H. & Jaluria, Y. 1995 Turbulent penetrative and recirculating flow in a compartment fire. *Trans. ASME J. Heat Transfer* **117**, 927–935.

Agrawal, A. & Prasad, A. K. 2004 Evolution of a turbulent jet subjected to volumetric heating. *J. Fluid Mech.* **511**, 95–123.

Becker, H. A. & Liang, D. 1978 Visible length of vertical free turbulent diffusion flames. *Combust. Flame* **32**, 115–137.

Becker, H. & Yamazaki, S. 1978 Entrainment, momentum flux and temperature in vertical free turbulent diffusion flames. *Combust. Flame* **33**, 123–149.

Bhat, G. S. & Narasimha, R. 1996 A volumetrically heated jet: large eddy structure and entrainment characteristics. *J. Fluid Mech.* **325**, 303–330.

Blake, T. R. & Coté, J. B. 1999 Mass entrainment, momentum flux, and length of buoyant gas diffusion flames. *Combust. Flame* **117**, 589–599.

Blake, T. R. & McDonald, M. 1995 Similitude and the interpretation of turbulent diffusion flames. *Combust. Flame* **191**, 175–184.

Cetegen, B. M., Zukoski, E. E. & Kubota, T. 1984 Entrainment in the near and far field of fire plumes. *Combust. Sci. Technol.* **39**, 305–331.

Chen, C. J. & Rodi, W. 1980 *Vertical Turbulent Buoyant Jets. A Review of Experimental Data.* Pergamon.

Dahm, W. J. A. 2005 Effects of heat release on turbulent shear flows. Part 2. Turbulent mixing layers and the equivalence principle. *J. Fluid Mech.* **540**, 1–19.

Dahm, W. J. A. & Dimotakis, P. E. 1987 Measurements of entrainment and mixing in turbulent jets. *AIAA J.* **25**, 1216–1223.

Delichatsios, M. 1987 Air entrainment into buoyant jet flames and pool fires. *Combust. Flame* **70**, 33–46.

Delichatsios, M. 1993 Transition from momentum to buoyancy-controlled turbulent jet diffusion flames and flame height relationships. *Combust. Flame* **92**, 349–364.

Gebhart, B., Jaluria, Y., Mahajan, R. L. & Sammakia, B. 1988 Buoyancy-Induced Flows and Transport. Hemisphere.

Han, D. H. & Mungal, M. G. 2001 Direct measurement of entrainment in reacting/non-reacting turbulent jets. *Combust. Flame* **124**, 370–386.

Hawthorne, W. R., Weddell, D. S. & Hottel, H. C. 1949 Mixing and combustion in turbulent gas jets. *Proc. Combust. Inst.* **3**, 266–288.

Heskestad, G. 1981 Peak gas velocities and flame heights of buoyancy-controlled turbulent diffusion flames. *Proc. Combust. Inst.* **18**, 951–960.

Hunt, G. R. & Kaye, N. G. 2001 Virtual origin correction for lazy turbulent plumes. *J. Fluid Mech.* **435**, 377–396.

Johnson, M. R. & Kostiuk, L. W. 2000 Efficiencies of low momentum jet diffusion flames in crosswinds. *Combust. Flame* **123**, 189–200.

Johnson, M. R. & Kostiuk, L. W. 2002 A parametric model for the efficiency of a flare in crosswind. *Proc. Combust. Inst.* **29**, 1943–1950.

Johnson, M. R., Spangelo, J. L. & Kostiuk, L. W. 2001 A characterization of solution gas flaring in Alberta. *J. Air Waste Man. Assoc.* **51**, 1167–1177.

Kaminski, E., Tait, S. & Carazzo, G. 2005 Turbulent entrainment in jets with arbitrary buoyancy. *J. Fluid Mech.* **526**, 361–376.

Karagozian, A. R. 1986 The flame structure and vorticity generated by a chemically-reacting transverse jet. *AIAA J.* **24**, 1502–1507.

Kotsovinos, N. E. & List, E. J. 1977 Plane turbulent buoyant jets. Part 1. Integral properties. *J. Fluid Mech.* **81**, 25–44.

Linden, P. F. 2000 Convection in the environment. In Perspectives in Fluid Dynamics (ed. G. K. Batchelor, H. K. Moffat & M. G. Worster). Cambridge University Press.

List, E. J. 1982 Turbulent jets and plumes. *Annu. Rev. Fluid Mech.* **14**, 189–212.

Mercier, G. D. & Jaluria, Y. 1999 Fire-induced flow of smoke and hot gases in open vertical enclosures. *Expl Therm. Fluid Sci.* **19**, 77–84.

Morton, B. R. 1958 Forced plumes. *J. Fluid Mech.* **5**, 151–163.

Morton, B. R. & Middleton, J. 1973 Scale diagrams for forced plumes. *J. Fluid Mech.* **58**, 165–176.

Morton, B. R., Taylor, G. I. & Turner, J. S. 1956 Turbulent gravitational convection from maintained and instantaneous sources. *Proc. R. Soc. Lond.* **234**, 1–23.

Mungal, M. G. & Hollingsworth, D. K. 1989 Organized motion in a high Reynolds number jet. *Phys. Fluids* A **1**, 1615–1623.

Muñiz, L. & Mungal, M. G. 2001 Effects of heat release and buoyancy on flow structure and entrainment in turbulent non-premixed flames. *Combust. Flame* **126**, 1402–1420.

Nguyen, T. T. & Karagozian, A. R. 1992 Liquid fuel jet in subsonic cross-flow. *J. Propust. Power* **8**, 21–29.

Papanicolaou, P. N. & List, E. J. 1988 Investigation of round turbulent buoyant jets. *J. Fluid Mech.* **195**, 341–391.

Peters, N. & Göttgens, J. 1991 Scaling of buoyant turbulent jet diffusion flames. *Combust. Flame* **85**, 206–214.

Steward, F. R. 1970 Prediction of the height of turbulent diffusion buoyant flames. *Combust. Sci. Technol.* **2**, 203–212.

Tacina, K. M. & Dahm, W. J. A. 2000 Effects of heat release on turbulent shear flows. Part 1. A general equivalence principle for nonbuoyant flows and its application to turbulent jet flames. *J. Fluid Mech.* **415**, 23–44.

Teixeira, M. A. C. & Miranda, P. M. A. 1997 On the entrainment assumption in Schatzmann's integral plume model. *Appl. Sci. Res.* **57**, 15–42.

Turner, J. S. 1986 Turbulent entrainment: the development of the entrainment assumption. *J. Fluid Mech.* **173**, 431–472.

Wohl, K., Gazley, C. & Kapp, N. 1949 Diffusion flames. *Proc. Combust. Inst.* **3**, 288–300.

Zukoski, E. E., Kubota, T. & Cetegen, B. 1981 Entrainment in fire plumes. *Fire Safety J.* **3**, 107–121.